이학박사 학위논문

Research of mechanism on effect of nitroxoline in a temozolomide—resistant glioblastoma: in vitro & in vivo experiments

테모졸로마이드 내성 교모세포종에서의 니트릭 솔린 효과 기반 메커니즘 연구

2021년 2월

서울대학교 대학원

의학과 협동과정 종양생물학 전공

Nisha Kumari

Ph.D. Dissertation of

Degree of Philosophy in Science

Research of mechanism on effect of nitroxoline in a temozolomide-resistant glioblastoma: in vitro & in vivo experiments

테모졸로마이드 내성 교모세포종에서 의 니 트릭솔린 효과 기반 메커니즘 연구

February 2021

Graduate School of Medicine

Seoul National University

Interdisciplinary Program in Cancer Biology

Nisha Kumari

테모졸로마이 드 내성 교모세 포종에서 의 니트릭솔린 효과에 대한 메커니즘 연구

지도교수 최숭홍

이 논문을 이학박사 학위논문으로 제출함

2021 년 02 월

서울대학교 대학원

의과대학 협동과정 종양생물학 전공

Nisha Kumari

NishaKumari의 박사학위논문을 인준함

2021 년 02월

위 원 장 김 인아 (인)

부 위 원 장 최 숭홍 (인)

위 원 우 홍표 (인)

위 원 박 천기 (인)

위 원 안 성수 (인)

Research of mechanism on effect of nitroxoline in a temozolomide-resistant glioblastoma- in vitro & in vivo experiments

Advisor : Seung Hong Choi

Submitting a Ph.D. Dissertation to Public Administration

February 2021

Graduate School of Medicine
Seoul National University

Confirming the Ph.D. Dissertation written by

Nisha Kumari

Chair In Ah Kim

Vice Chair Seung Hong Choi

Examiner Hong Hyun Ku

Examiner Chul-Kee Park

Examiner Sung Soo Ahn

Abstract

Research of mechanism on effect of nitroxoline in a temozolomide-resistant glioblastoma* in vitro & in vivo experiments

Nisha Kumari

Interdisciplinary Program in Cancer Biology

Graduate School of Medicine

Seoul National University

Background: Glioblastoma multiforme (GBM) is one of the most devastating primary malignant brain tumors and remains a major challenge in oncology. The current standard of care for GBM includes safe surgical resection, radiotherapy and chemotherapy. In chemotherapy, temozolomide (TMZ) is the standard of care for GBM patients. However, a large percentage of tumors are resistant to the cytotoxic effects of the TMZ-induced DNA lesion 06-methylguanine due to elevated expression of the repair protein 06—methylguanine—DNA methyltransferase (MGMT) or a defect in the mismatch repair (MMR) pathway. Although, a majority of the TMZ-induced lesions (N7—methyleguanine and N3-methyleadenine) are base excision repair (BER) substrates, these DNA lesions are readily repaired, therefore the BER proteins are attractive target for reversing TMZ-resistance. In our study, I focused on the apurinic / apyrimidinic

endonuclease—1 (APE-1), a multifunctional enzyme, involved in the BER pathway.

Material & methods : Here, I generated TMZ-resistant cell lines in vitro and evaluated the therapeutic effects of nitroxoline (NTX) in TMZ-resistant cell line by clonogenic and migration assay. I used quantitative RT-PCR to investigate the expression level of proteins associated with TMZ-resistance in TMZ-resistant cell lines before and after nitroxoline (NTX) treatment. I also performed flow cytometry and western blot in in vitro. In in vivo study, I prepared TMZ-resistant GBM mouse model and performed 9.4T MRI to obtain T2WI and DWI for assessment of tumor volume and changes in ADC value respectively. Lastly, I perform histological analysis and regression analysis to investigate the relationship between ADC and histological findings.

Results: I observed the significantly decreased expression of APE-1 after NTX treatment which trigger apoptosis in TMZ-resistant cells. I also observe that NTX significantly reduced the colony forming capacity and migration capacity of TMZ-resistant cells. In in vivo study, NTX reduced the tumor growth in TMZ-resistant GBM mice. Moreover, ADC was increased in NTX—treated TMZ-resistant GBM mice as compared to non-treated group, which was prior to tumor volume decrease. The decreased expression of APE-1 by NTX leads to therapeutic effects and is inversely correlated with ADC in TMZ-resistant GBM, which results in longer survival in NTX treated animals.

Conclusion : NTX could induce apoptosis through the decreased expression of APE—1 in TMZ-resistant GBM in vitro and inhibit the growth of a TMZ-resistant GBM tumor model. Therefore, NTX is suggested as potential

therapeutic candidate against TMZ-resistant GBM.

Parts of the results in this thesis have been published in the following papers:

Hye Rim Cho* Nisha Kumari*, Nishant Thakur, Hien Thi Vu, Hyeonjin Kim, Seung Hong Choi. Decreased APE-1 by Nitroxoline Enhances Therapeutic effects in a temozolomide-resistant Glioblastoma* Correlation with diffusion-weighted imaging. Scientific Reports 2019:12:16613.

Conference: Poster presentations from this thesis:

22nd Annual meeting and education day of the Society for Neurooncology, November2017, Marriott Marquis, San Francisco, California. DDIS-04 Nitroxoline exhibit anticancer activity inducing apoptosis in a temozolomide-resistant glioblastoma. Neuro-oncology, 06 Nov 2017, 19(Suppl 6) :vi59_vi59.

Keywords: Temozolomide-resistant glioblastoma, DNA-repair protein, Base excision repair (BER), apurinic/apyrimidinic endonuclease —1 (APE-1), nitroxoline (NTX), diffusion-weighted imaging (DWI), apparent diffusion coefficient (ADC)

Student Number: 2016 — 30782

List of Contents

List of Figures

List of Tables

Abbreviations*.

GBM	Glioblastoma
TMZ	Temozolomide
NTX	Nitroxoline
FDA	Food & drug administration
WHO	World Health Organization
MRI	Magnetic resonance imaging
DWI	Diffusion—weighted imaging
ADC	Apparent diffusion coefficient
DNA	Deoxy ribonucleic acid
MGMT	06—methylguanine-DNA methyltransferase
MMR	Mismatch repair
BER	Base excision repair
BBB	Blood brain barrier
MTIC	Methyle — 1 —triazenoimidazole—4—carboxamide
RTK	Receptor tyrosine kinase
MetAP2	Type 2 methionine aminopeptidase
SIRT1	Sirtuin-1
ECM	Extracellular matrix
PARP	Poly (ADP-ribose) polymerase
DMSO	Dimethyl sulfoxide
FBS	Fetal bovine serum
DMEM	Dulbecco' s modified eagle medium
RPMI	Roswell park memorial institute medium

PBS	Phosphate buffered saline
BSA	Bovine serum albumin
DAPI	Diamidino —2-phenylindole
CCK	Cell counting kit
RRAD	Ras associated with diabetes
RT-PCR	Reverse transcription-polymerase chain reaction
cDNA	Complementary DNA
siRNA	Small interfering RNA
MSH-2	MutS protein homolog 2
MSH-6	MutS protein homolog 6
Cx43	Connexin 43
APNG	Alkylpurine - DNA-N—glycosylase
APE1	Apurinic/apyrimidinic endonuclease — 1
IQR	Interquartile range
DAB	Di amino benzidine
EMT	Epithelial-mesenchymal transition
PI3K	Phosphatidylinositol-3-kinase
TUNEL	Terminal deoxy nucleotidyl transferase-mediated dUTP nick-end labeling

1. Introduction

1.1 Background

Glioblastoma multiforme (GBM) is the most devastating primary malignant brain tumor accompanied by poor prognosis and high lethality. According to neuropathological classification schemes, it has been graded as WHO grade IV brain tumors (1). The prognosis and survival of GBM patients remain poor, accompanied by median survival of about 12 to 14 months (2). The current standard therapy is surgical resection followed by radiotherapy plus temozolomide (TMZ). The foundation in the early treatment for malignant glioma is surgery which results in decreased tumor burden and mass effect. GBM resection is directed at maximal safe resection and it has been reported to extends the survival in GBM patients. Generally, radiotherapy improves the survival benefits in glioma patients. The radiotherapy damages DNA in mitotically active cells. Cancer cells are incompetent to handle DNA damage and ultimately decline the mitotic activity and die (3). According to Stupp et. al, the standard treatment regimen for GBM patients involves the surgical resection followed by radiotherapy plus TMZ (4, 5). TMZ is an DNA-methylating agent, 100% bioavailable which, due to its lipophilic nature, readily crosses the blood brain barrier (BBB). Glioblastoma patients who initially respond to TMZ will inevitably undergoes a relapse during or after its cessation. When therapy reaches a plateau due to chemo-resistance, understanding the mechanisms of this event becomes critically important in overcoming this major clinical challenge. To overcome the TMZ-resistance, various studies have reported the mechanism of development of TMZ—resistance. The best—reported mechanism

of TMZ—resistance is mediated by MGMT, a DNA repair protein, which eliminates methyl groups from O6-guanine position that arise from TMZ treatment (6). Although O6-meG is the least frequently alkylated (8%) and major cytotoxic DNA adduct induced by TMZ. Previous studies reported that the cell lines with higher levels of MGMT showed increased resistance to TMZ and inhibition of MGMT downregulated the resistance and upregulated the sensitivity to TMZ treatment (7, 8). Excluding MGMT-mediated direct DNA repair, all other repair systems involve the recognition and excision of the damaged nucleotide with the possible inclusion of its immediate surrounding area, followed by DNA resynthesis. One such mechanism involves MMR, which maintains genomic stability by identifying and correcting mispaired nucleotide bases that escaped proteasomal proofreading during DNA replication. In tumors with MGMT deficiency, O6-meG persists and mispairs with thymine. In an attempt to restore this anomaly, the MMR system is activated and excises thymine from the daughter DNA strand leaving the O6-meG adduct on the template strand intact. This process initiates repetitive cycles of futile repair involving thymine reinsertion and excision, leading to successively longer DNA resections, the accumulation of double-strand breaks, and ultimately apoptotic tumor cell death (9). Therefore, glioblastomas with an intact MMR process with low MGMT expression are considered the most sensitive to TMZ (Figure 1). Whereas, MMR is principally involved in repair of DNA replication error, base excision repair (BER) has been reported as a major pathway involved in repairing damaged DNA caused by alkylating agent induced lesions (10, 11). The bulk of methylated DNA adduct (more than 90%) is comprised of either

N7-meG or N3-meA which are substrates of BER system. The retrospective review of high-grade glioma specimens concluded that the higher expression of APE-1 was associated with tumor progression and confers resistance to ionizing radiations and DNA methylating agents (12, 13).

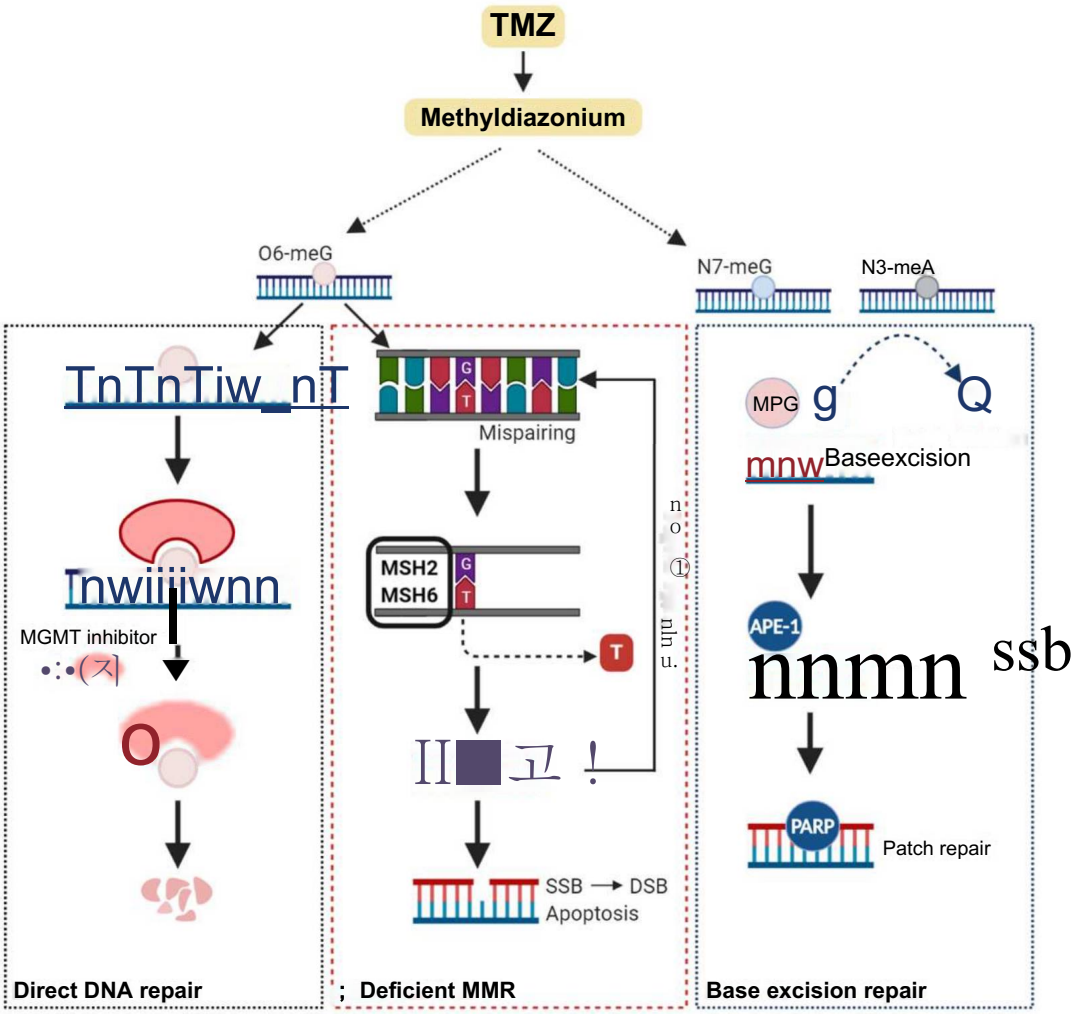

Figure 1. DNA repair mechanisms deal with DNA damage produced by TMZ. TMZ cleaved into active methyldiazonium salts, which methylates DNA guanine residues at the 06 (06-meG) and N7 (N7-meG) positions as well as adenine at the N3 (N3-meA). The 06-meG is rapidly neutralized by MGMT and restore DNA integrity by direct repair. N7-meG and N3—meA DNA adducts are efficiently repaired by MMR and BER pathway.

(Figure adapted from Arora et. al doi: 10.1080/15384047.2019.1599662)

The de novo development of new medicines takes lot of time and cost. The drug repurposing represents an alternative way of improving the rate of success, shortening the processing time, and trimming costs of cancer drug development (14, 15). Nitroxoline (NTX), is an FDA-approved antibiotic against urinary tract infections that have been repurposed for cancer treatment. The antimicrobial activity mode of action of the NTX is related mainly to its ability to chelate with Mg^{2+}, stabilizing the lipopolysaccharide molecules that form the outer bacterial membrane which decrease adherence capacity. Due to its long time use in clinical practice, the pharmacokinetic and pharmacodynamic properties of NTX are well established (16). The antitumor activity of NTX was identified in a search for Type 2 methionine aminopeptidase (MetAP2) inhibitors as novel antiangiogenic agents by Shim et. al. (17). MetAP2 is a ubiquitously expressed intracellular metallopeptidase and has been identified as an important molecular target for angiogenesis inhibitors which are able to suppress endothelial cell proliferation (18). Sirtuin-1 (SIRT1) is a component of the sirtuins family that regulates histone deacetylation and has a critical repressive effect on tumor suppressor p53 and other stress regulated genes, during cancer progression (19). Inhibition of SIRT1 promotes premature death of endothelial cells and therefore, identified as a promising target for inhibition of angiogenesis (19). The study of Shim and others shows that NTX is a potent inhibitor of MetAP2 in vitro, thus inhibiting endothelial cellular proliferation and tube formation, both in vitro and in vivo (17). Moreover, it reduces tumor volume in breast cancer xenografts and inhibits the growth of bladder cancer as shown in an orthotopic mouse model. Further, NTX inhibits SIRT1 and induces

an increase in the level of acetylated p53. Thus, NTX is a dual inhibitor of MetAP2 and SIRT1, with the synergistic effect of inducing senescence and inhibiting HUVEC proliferation and suggested as a potent inhibitor of angiogenesis (17). NTX was identified as a potent and reversible non-covalent inhibitor of cathepsin B. Cathepsin B is a lysosomal cysteine peptidase which acts as a tumor-promoting factor, contributing to the degradation of extracellular matrix (ECM), a crucial step that promotes tumor migration and invasion and enables metastasis and angiogenesis (20). Previous researcher reported that NTX inhibits cathepsin B endopeptidase activity and significantly reduces the degradation of ECM, tumor cell invasion, and endothelial tube formation in vitro in a number of cell lines and significantly abrogates tumor growth and metastasis in vivo in tumor mice models (21). Further, NTX has been found to induce G0/G1 arrest which results in apoptosis via the increased expression of cleaved caspase 3 and cleavage of poly (ADP-ribose) polymerase (PARP) in PTEN/KRAS glioma in vivo in a genetically engineered mouse glioma model (22). The effect of NTX on cell-cycle arrest and apoptosis was also confirmed in prostate cancer cells in which it induced G1 cell-cycle arrest on both hormone - sensitive and hormone-refractory prostate cancers.

In this study, researchers showed that NTX treatment induces G1 cell-cycle arrest in prostate cancer cells by inhibiting the cyclin Dl-Rb-Cdc25A axis that is responsible for the progression of the G1 phase of the cell cycle and activate AMPK and thus inhibiting the downstream effector mTOR signaling pathway (23). NTX also shown to downregulated expression of programmed death-ligand 1 (PD-L1) in prostate cell lines and in tumor tissue. The effect of NTX

on a murine orthotopic model of RM9—Luc-PSA prostate cancer was assessed together with the effect of PD-1 blockade. Additionally, combination treatment was also suggested to enhance antitumor immunity, causing increased numbers of $CD44^+CD62L^+CD8^+$ memory T cells and a reduction in the number of immunosuppressive myeloid—derived suppressor cells (MDSCs) in peripheral blood of C57BL/6 mice (24). Therefore, based on history of NTX as a safest compound and its ability to suppress cancer, I speculated that it has the capability to be used against GBM.

Diffusion-weighted imaging (DWI) is a promising technique to evaluate the response to treatment in tumors in both clinical and research settings. The lot of research studies are currently ongoing or published on the use DWI as a prognostic marker in different types of cancer (25). ADC is a measurement of the magnitude of diffusion of water molecules within cells and are calculated by software and then laid out as parametric map that reflects the level of water diffusion through different tissues and expressed in units of mm^2/s. The apparent diffusion coefficient (ADC) is a measured from DWI is sensitive to the tumor microenvironment and is a potential noninvasive biomarker for the prediction and monitoring of the response to therapy (26, 27). ADC maps can provide valuable information as they reflect the mobility of water molecules within the tissues and can sensitively detect changed cellularity in tumors (28). Sugahara et al. reported that the ADC is negatively correlated with the tumor cellularity, with a high cell density and extracellular tortuosity resulting in an increased restriction of the diffusion of water molecules (29). Considering all these findings, the purpose was to investigate the therapeutic effects of NTX

against TMZ-resistant cancer cell lines in vitro and in vivo in a TMZ-resistant GBM bearing mouse model by using DWI.

1.2 Purpose of Research

The main objective of this study was to investigate the therapeutic effects of NTX in TMZ-resistant glioblastoma. In vitro study was designed to demonstrates the effect of NTX on proliferation, migration capacity and on expression of proteins associated with TMZ—resistance in TMZ-resistant cell lines. In in vivo, the purpose was to check whether NTX has the potential to reduce tumor volume and increase the ADC value in a TMZ-resistant GBM bearing mouse model.

2. Material and Methods

2.1 Cell culture

The human GBM cell lines LN229 and U87 MG were chosen for my study and purchased from the American Type Culture Collection. The LN229 cells were cultured in Dulbecco' s modified eagle medium (DMEM) and U87 cells were cultured in Roswell park memorial institute medium (RPMI), both medium were supplemented with 10% fetal bovine serum (FBS) and 5% penicillin / streptomycin at 37° C in the presence of 5% CO2. These cell lines were designated the parental cell lines.

2.2 TMZ-resistant GBM cell lines

TMZ—resistant cell lines (LN229R and U87R) were established from the parental cell lines by continuously exposing the LN229 and U87 cancer cell lines to low doses of TMZ starting from 5 // M and increasing to 40 // M for 10 months. The half-maximal inhibitory concentration (IC50) was used to measure the cytotoxicity of TMZ and to compare the TMZ—resistant cell lines with the parental cell lines. The half-maximal inhibitory concentrations (IC50) for both cell lines were different before and after treatment.

2.3 Cytotoxicity assay

The cell counting kit—8 (CCK-8, Dojindo) was used to measure cell viability following NTX treatment. LN229R and U87R were plated (5000 cells/well) in 96-well plates. The TMZ-resistant cells were cultured for 24 hours in CO2 incubator in a medium containing 1% DMSO for the control or 10, 15, 20 // g/ml

NTX for the treatment groups. After incubation with NTX/DMSO, the cells were incubated with CCK-8 for 1 hour at 37° C. The total amount of formazan formed by the viable cancer cells was measured by the absorbance at 450 nm by using the synergy Hl plate reader (Tecan Sunrise TW). The number of viable cells at different NTX concentrations is expressed as a percentage of the control cells. All experimental conditions were carried out in sextuplicate.

2.4 Colony formation assay

Clonogenic survival assays was performed by seeding TMZ-resistant cells (1000 cells/2 ml) in 6-well plates. In this assay, experimental groups were treated with 0.5 "g/ml NTX and the control group was supplemented with medium containing TMZ. All groups were observed for 10 days. The doubling times for U87 and LN229 was approximately 32 hours and 24 hours respectively. After 10 days, the cells were fixed with 4% paraformaldehyde and stained with 0.5% crystal violet solution at room temperature. The cell density was evaluated by crystal violet staining of the adherent cells. The colony formation inhibition rate was calculated with the following formula* .

plating efficiency = number of colonies counted / number of cell plated x 100%.

2.5 Migration assay

The cell migration capacity was investigated using the Ibidi culture-insert 2-well plates (Ibidi, Bonn). The culture inserts consisted of two wells separated by a 500-mm thick wall. The same amount of cell suspension (5 x 10^5 cells/ml) was dispensed in each plate, including each well, followed by incubation in a CO2

incubator at 37° C. After approximately 6 to 8 hours, when the cells had attached completely, the cells were gently treated with either 10 "g/ml NTX or culture medium. To investigate the migration capacity of cells, the wall was removed very gently under aseptic conditions, and that time point was considered 0 hours. After 24 and 48 hours of treatment, the space between two cell layers was observed under a microscope. All experiments were carried out in quadruplicate.

2.6 Immunofluorescence analysis

TMZ-resistant cells (lxlO^5) were seeded on glass cover slips for 24 hours and treated with 10 // g/ml NTX (experimental group) or 1% DMSO (control group) for 24 hours. After 24 hours, the cells were fixed in 4% formaldehyde for 15 minutes at 37° C and permeabilized for 10 min in 0.1% Triton X-100. After washing with PBS, the cells were incubated with BSA for 30 minutes for blocking. The cells were incubated with anti-tubulin primary antibody (1÷100, Sigma Aldrich) for 1 hour at room temperature. After rinsing with PBS, the cells were stained with a secondary antibody (Alexa Fluor 594 goat anti-mouse IgG, Invitrogen) for 1 hour and mounted with 1 // g///1 DAPI. For fluorescence imaging, the cells were observed under a fluorescence microscope (LEICA CTR5500), and all images were captured under same parameters.

2.7 Flow cytometric analysis of PI staining

LN229R and U87R (lxlO^5) cells were seeded in DMEM and RPMI media and treated with 10 사 g/ml NTX (dissolved in culture medium) for 24 hours at

37° C in a CO2 incubator. The cells were harvested by trypsanization, fixed by incubation in 70% (v/v) alcohol at 4° C for 30 minutes and washed with PBS. The cells were centrifuged and resuspended in 10 //1 of propidium iodide (1 mg/ml) solution containing RNAse (10 mg/ml). The DNA content was measured with a FACS scan flow cytometer.

2.8 Western blotting

The TMZ-resistant cells ($1x10^5$) were seeded and treated with 10 |ig/ml NTX for 24 hours. For the western blot analysis, 50 "g/ml proteins were loaded onto the gel, and the following primary antibodies were used- anti-cyclin DI (Santa Cruz Biotechnology), anti-Ph-Rb (Cell Signaling Technology), anti-cyclin A (Santa Cruz Biotechnology), anti-CDKl (Abeam), anti-cleaved caspase-3 (Cell Signaling Technology), anti-poly (ADP-ribose) polymerase (PARP) (Cell Signaling Technology), anti-Ras associated with diabetes (RRAD) (Abeam), anti-GAPDH (Santa Cruz Biotechnology), and anti-β-actin (Abeam). All primary antibodies were detected by horseradish peroxidase-conjugated secondary antibodies (Santa Cruz Biotechnology). The band intensities were quantified using ImageJ software.

2.9 Reverse transcription-polymerase chain reaction (RT-PCR) analysis

RNA was extracted with TRIzol reagent (Invitrogen). Reverse transcription was performed using the high capacity cDNA reverse transcription kit (Life Technologies-Applied Biosystems) in accordance with the manufacturer's recommendations. Real-time PCR was performed with 1 // g of cDNA on a CFX

Connect Real-Time PCR (BIORAD) using iQ SYBR green. The initial incubation was at 65° C for 10 minutes. The primer sequences used in the PCR were as follows- Apurinic/apy rimidinic endonuclease (APE—1): (F) 5' — TTGTGGCTGAATTTGACTCG-3 ' (R) 3 ' -TTGAGGTCTCCACACAGCAC-5 ', MutS protein homolog 2 (MSH—2): (F) 5 ' — GCC ATTTTGGAGAAAGGAC A- 3 ' (R) 3 " - CTC AC ATGGC AC A A A AC ACC - 5 ', MutS protein homolog 5 (MSH-6)- ' (F) 5 ' — GATTCCATTGGGTTGACACC-3' (R) 5"-AGCACCATTCGTTGATAGGC-3 O^{6}-alkylguanine DNA alkyl transferase (MGMT): (F) 5'-GTGGCCTCACGATGTGTATG -3 ^{7} (R) 3 ' - ACCCGCTGTGTGACTTATCC-5 " and connexin 43 (Cx43) : (F) 5 ^{z} - ATGAGCAGTCTGCCTTTCGT-3' (R) 3 " -TCTGCTTCAAGTGCATGTCC-5 ' . All primers were purchased from Bioneer. The relative expression was calculated using 2 (AACT).

2.10 Live and dead cell detection assay

The live and dead cell detection assay was performed using the live and dead cell detection assay kit (Abeam), which determines intracellular esterase activity and plasma membrane integrity, both of which are considered hallmarks of viable cells. Live cells were identified based on the intracellular esterase activity and the exclusion of the red dye, resulting in green fluorescence. Dead were detected based on the lack of esterase activity and non-intact membranes, resulting in red fluorescence. Briefly, TMZ—resistant cancer cells (lxlO^{5}) were treated with 10 "g/ml NTX for 24 hours and stained with the live and dead cell

detection reagents before being incubated at 37° C for 10 minutes. The slides were analyzed under a fluorescence microscope (LEICA CTR5500).

2.11 TMZ-resistant GBM mouse model

This study was approved by the institutional animal care and use committee of Seoul National University Hospital. All research was performed in accordance with the relevant guidelines/regulations in our institute (16-0130-C1A0). To prepare the xenograft GBM mouse model, 6-week—old male nude mice (z? = 12) were anesthetized by the intraperitoneal injection of a mixture of Zoletil (zolazepam) and Rompun (xylazine) and were placed in a stereotaxic device. The mice were inoculated with LN229 glioma cells ($3xl0^6$ cells/3 //l). The cells were injected in the caudate/putamen region of the brain by using a Hamilton syringe fitted with a 28-gauge needle, which was positioned with a syringe attachment fitted to the stereotaxic device. Two weeks after tumor implantation, the required tumor size was confirmed by pretreatment MRI (Pre-MRI). For TMZ—resistant models, GBM—bearing mice were developed by administering successive high doses of TMZ (100 mg/kg/day) intraperitoneally until tumor growth showed no inhibition by TMZ for 7 days, as described in previously reported studies (30-32). The models were further confirmed by post—1 MRI including T2WI for the assessment of tumor size.

2.12 Short-term in vivo treatment response study in a TMZ-resistant GBM mouse model

For the short-term treatment response study, we divided the animals into 3 groups after the confirmation of TMZ-resistance by post—1 MRI. Four TMZ—resistant GBM mice were intraperitoneally injected with 1% saline for 7 days (control group). The four TMZ—resistant GBM mice were intraperitoneally treated with 100 mg/kg/day of NTX for 7 days (NTX group). The remaining four TMZ—resistant GBM mice were intraperitoneally treated with 100 mg/kg/day of TMZ for 7 days (TMZ group). The post-2 MRI was conducted after the saline or NTX or TMZ treatment to evaluate the therapeutic effects on tumor growth. DWI was also acquired sequentially.

2.13 MRI protocol and analysis

For the in vivo animal MRIs, the animals were anesthetized with 1.5-2% isoflurane/oxygen (v/v), and then scanned by using a 9.4T MR scanner (Agilent Technologies, Santa Clara, CA, USA). Throughout each imaging session, the animals were wrapped in warm water blankets, and their oxygen saturation and heart rates were monitored. In the T2WI in the coronal plane, fast spin-echo multi—slices methods were employed (TR = 3000 ms, effective TE = 31.18 ms, ETL = 4, average = 2, data matrix size = 256 x 256, and FOV (field of view) = 25.0 x 25.0 mm^2). The echo-planar DWI in the coronal plane was also obtained (TR/TE = 4000/60.04 ms, with shots = 2, repetitions = 1, average = 2, matrix = 128 x 128, FOV = 24.0 x 24.0 mm^2, b—value = 0, 100, 200, 400, 700 and 1000 s/mm^2, 1 mm slice thickness). In addition, apparent diffusion coefficient (ADC) maps were generated, and image analysis was performed by

using our in-house software developed with a commercial analysis package (MATLAB version R2007b, MathWorks Inc., Natick, MA, USA).

I drew the regions of interest (ROIs) that contained the entire tumor on every continuous section of the coregistered T2WI and ADC maps. Tumor boundaries were defined with reference to the high-signal intensity areas thought to represent tumor tissue on the T2WI. Finally, I calculated the tumor volume and mean ADC for each tumor, as well as the ratios of the tumor volumes and the ADC values (post-2 value/post-1 value x 100).

2.14 Long-term survival analysis in a TMZ-resistant GBM mouse model

For the long-term survival analysis of 70 days, we used TMZ-resistant GBM mice(77 = 18) generated by a previously described method (30-32). The mice were divided into two groups [control, (n = 9, saline-treated) and NTX, (、n = 9)] according to tumor sizes, which were equally distributed in each group. The saline solution or NTX were injected in the same manner as described above (Material and method, 2.12) in the control and NTX groups, respectively, during the follow-up period. All mice were observed until euthanasia or the survival endpoint of 70 days.

2.15 Immunohistology

For immunohistological analysis, all animals were sacrificed and perfused with normal saline after performing MRI. The brain tissues were extracted, preserved in 10% formalin and embedded in paraffin. I prepared 4 // m thick tissue sections and stained then with the primary antibody against APE-1 (for

DNA—repair*, Novus biologicals) and Ki—67 (for cancer cell proliferation; UltraMab) as primary antibodies. Then, the sections were rinsed with washing buffer and incubated with horseradish peroxidase-conjugated secondary antibodies (Santa Cruz Biotechnology) for 30 minutes at room temperature. Staining for the detection of the bound antibodies was evaluated by DAB. Additionally, brain tumor sections were also subjected to a TUNEL assay to measure the degree of DNA strand breaks, a hallmark of apoptosis.

2.16 Statistical analysis

All statistical analyses were performed using MedCalc Software (MedCalc version 13.1.0.0). The Kolmogorov-Smirnov test was used to determine the normal distribution of the noncategorical variables. The nonparametric data are presented as the median and interquartile range (IQR, range from the 25th to the 75th percentile), and the parametric data are shown as the mean ± standard deviation. According to the results of the Kolmogorov-Smirnov test, a paired or unpaired Student's t-test, Mann-Whitney U~test or Wilcoxon test was performed, as appropriate, to compare the values between two groups. Survival data in the GBM mouse model were analyzed by using the Kaplan-Meier with a log rank method and the Cox proportional hazards model in the GBM mouse model.

3. Results

3.1 Generation of TMZ-resistant cells

I generated TMZ—resistant GBM cell lines (U87R & LN229R) for the in vitro study. The IC50 was 3.4-fold greater in the LN229R cells than in the LN229 cells, reaching 124 // M in LN299R, compared to 37 // M in LN229 (Figures 2A & 2B). The IC50 was 1.7-fold greater in U87R than in U87, reaching 82 //M in U87R compared to 48 "M in U87 (Figure 2C). Yeom et. al. reported that the increased expression of RRAD (Ras associated with diabetes) are associated with TMZ-resistance in glioblastoma cell lines (33). I also confirmed the resistance level in our cell lines by investigating the increased protein expression of RRAD in both TMZ—resistant cell lines (Figure 2D & 2E).

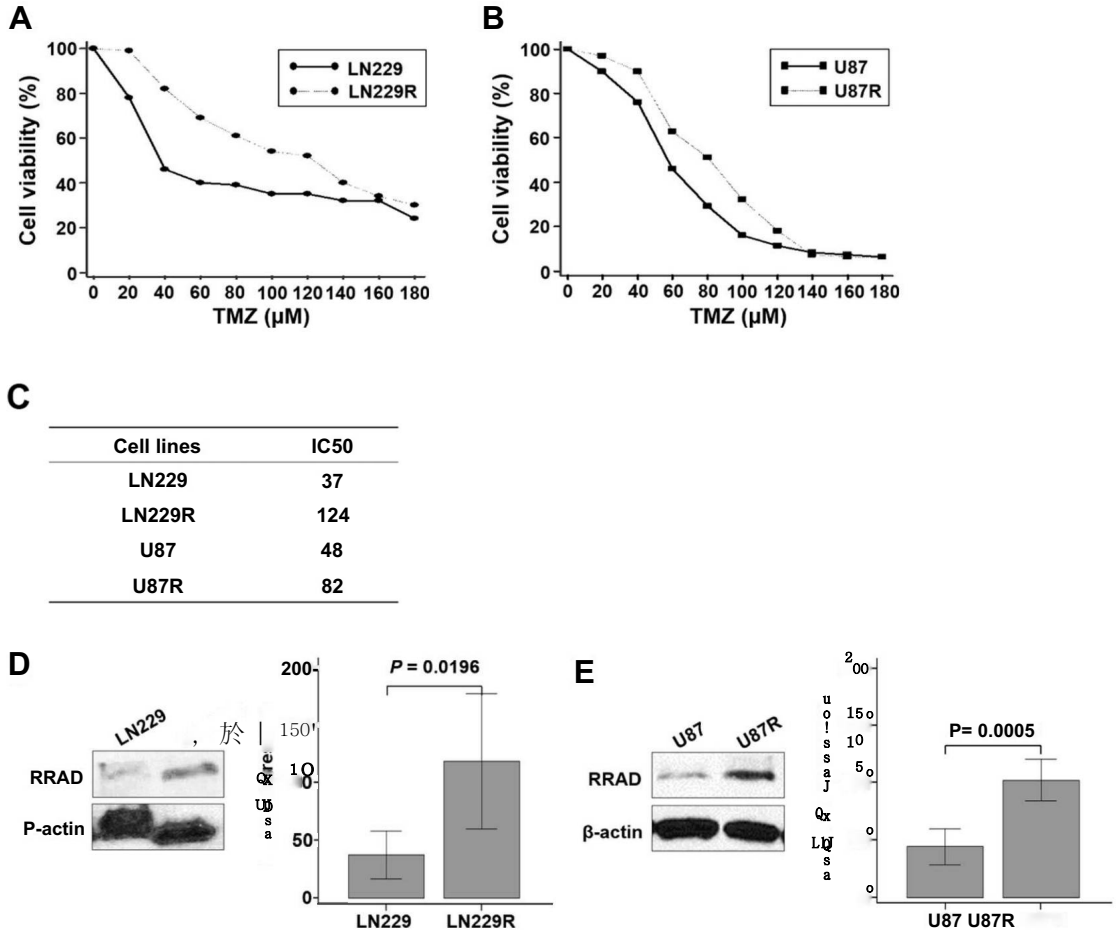

Figure 2. Generation of TMZ-resistant cells. Generation of TMZ-resistant (A) LN229R and (B) U87R GBM cell lines by continuously exposing parental cell lines with low doses of TMZ starting from 5 서 M to 40 "M for 10 months. (C) IC_{50} of TMZ-resistant cells was 3.4-folds higher than that of the parental cells in LN229R and nearly 1.7—folds higher in U87R. RRAD expression of (D) LN229R and (E) U87R GBM cells significantly increased than those of parental cells as analyzed by western blot analysis (LN229 vs. LN229R ; P = 0.0196, and U87 vs. U87R ; P= 0.0005).

3.2 NTX reduced the cell proliferation in parental cells as well as TMZ-resistant cancer cells

To evaluate the therapeutic effects of NTX in vitro, first I checked the effect of NTX on cell viability of LN229 and U87 cells with various concentration of NTX (20, 40, 60, 80, 100, and 120 // g/ml) for 24 hours. I observed that NTX treatment for 24 hours decreased the cell viability in both parental cell lines (Figure 3A) and further I decided to investigated the effect of NTX on cell viability in both TMZ-resistant GBM cell lines. I also observed the decreased cell viability with different concentration (10, 15, and 20 //g) of NTX in both TMZ-resistant cell lines (Figure 3B). This data show that NTX treatment inhibits cell proliferation in both parental cell as well as TMZ-resistant GBM cells.

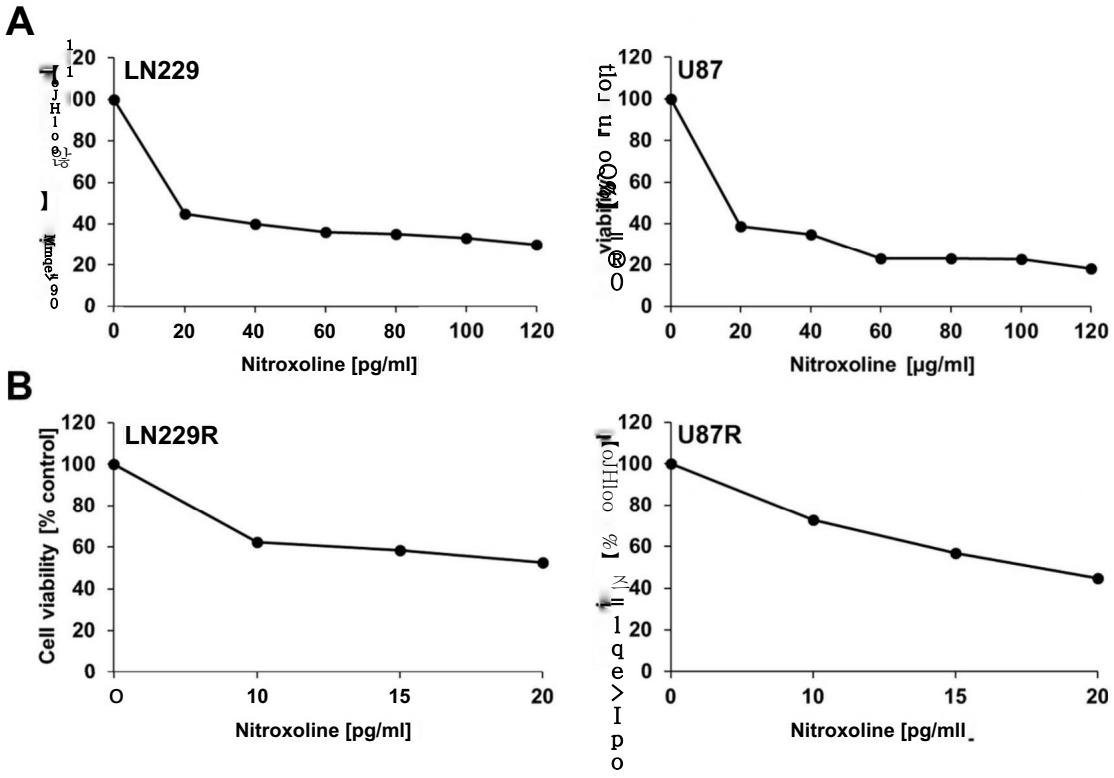

Figure 3. Effect of NTX on cell viability inhibition of parental and TMZ-resistant cells. Cell viability inhibition of (A) parental cells (LN229 and U87) and (B) TMZ-resistant cells (LN229R and U87R) by NTX in a dose—dependent manner.

3.3 NTX treatment recovers cell morphology change and inhibits colony formation and migration in TMZ-resistant GBM cells

TMZ-resistance induced morphological transformations in both of the resistant cell lines as the cells changed from round or oval shapes to elongated and spindle shapes, as demonstrated by a -tubulin staining under a fluorescence microscope (Figure 4A). However, the cytoskeleton was disrupted and recovered to the original parental morphology after 10 나 g/ml of NTX treatment for 24 hours in both of the TMZ—resistant cell lines (Figure 4B). To evaluate the therapeutic effects of NTX in vitro, I performed a colony formation and migration assay. NTX (0.5 사 g/ml) significantly reduced the formation of colonies in both of the TMZ-resistant cell lines after 10 days of treatment. Approximately 60% and 80% of the colonies were inhibited in TMZ-resistant LN229 (LN229R)(P= 0.0180) and TMZ-resistant U87 (U87R) (P= 0.0172), respectively (Figure 4C). In a migration assay, I found that 10 jig/ml of NTX inhibited approximately 84% and 80% of the migration over 48 hours in LN229R (P = 0.0180) and over 24 hours in U87R (P= 0.0180), respectively, when compared to their respective nontreated groups (Figure 4D).

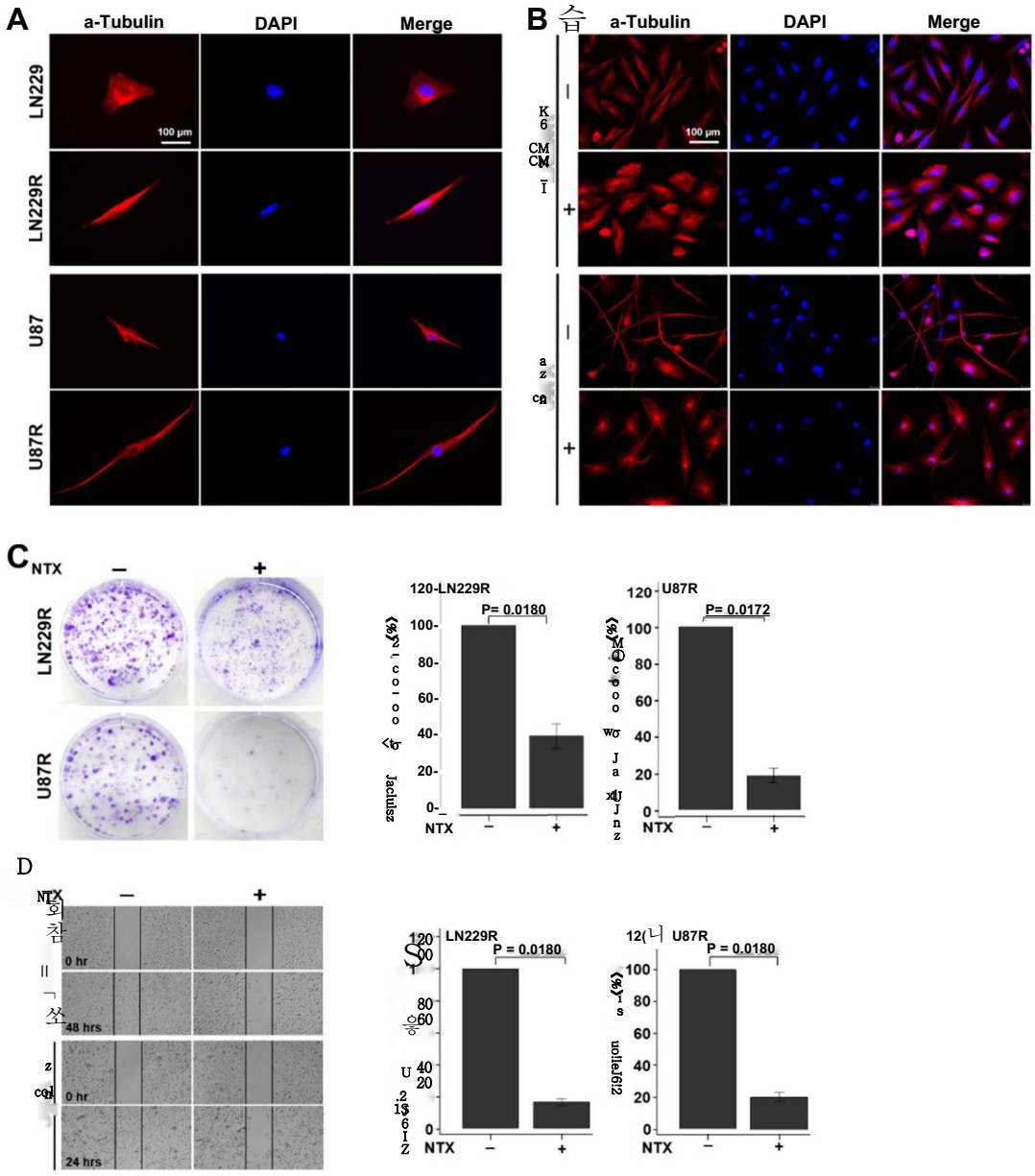

Figure 4. NTX restored changes in cell morphology and inhibited colony formation and migration in TMZ—resistant GBM cells. (A) Immunofluorescence images of TMZ-resistant GBM cells and their respective parental cells to compare the morphological differences before and after TMZ treatment. The parental cells changed their morphology from a round or oval shape to a dendritic shape after TMZ treatment in both cell lines. Magnification: x 400. (B) The morphology of LN229R and U87R cells recovered as parental cells after NTX treatment.

Magnification : x 200. (C) Colony formation was significantly decreased in LN229R (戶 = 0.0180) and U87R CP = 0.0172) cell lines after NTX treatment. (D) The migration capacity was also significantly reduced in LN229R after 48 hours (P = 0.0180) and in U87R after 24 hours (、P = 0.0180) after NTX treatment. Note- LN229R = TMZ—resistant LN229 and U87R = TMZ—resistant U87.

3.4 Effects of NTX treatment on cell-cycle

To scrutinize the internal mechanism by which NTX inhibits cell proliferation, the flow cytometry analysis of the DNA content was performed in LN229R and U87R cells treated with 10 나 g/ml NTX for 24 hours. Representative cell-cycle profiles are shown in Figure 5. Treatment with NTX induced a significant increase in the percentage of cells at the G0/G1 phase and a decrease in the percentage at the G2/M phase of the cell cycle. In detail, a significant proportion of cells were observed in G0/G1 phase [LN229R- 65% ± 3.28 (、P = 0.0286) ; U87R÷ 74% ± 0.87,€P0.0286)]. In addition, the percentage of cells in the G2/M phase was significantly decreased [LN229R- 5% ± 0.83 (、P = 0.0286) ; U87R： 6% ± 0.64 (戶 = 0.0286)].

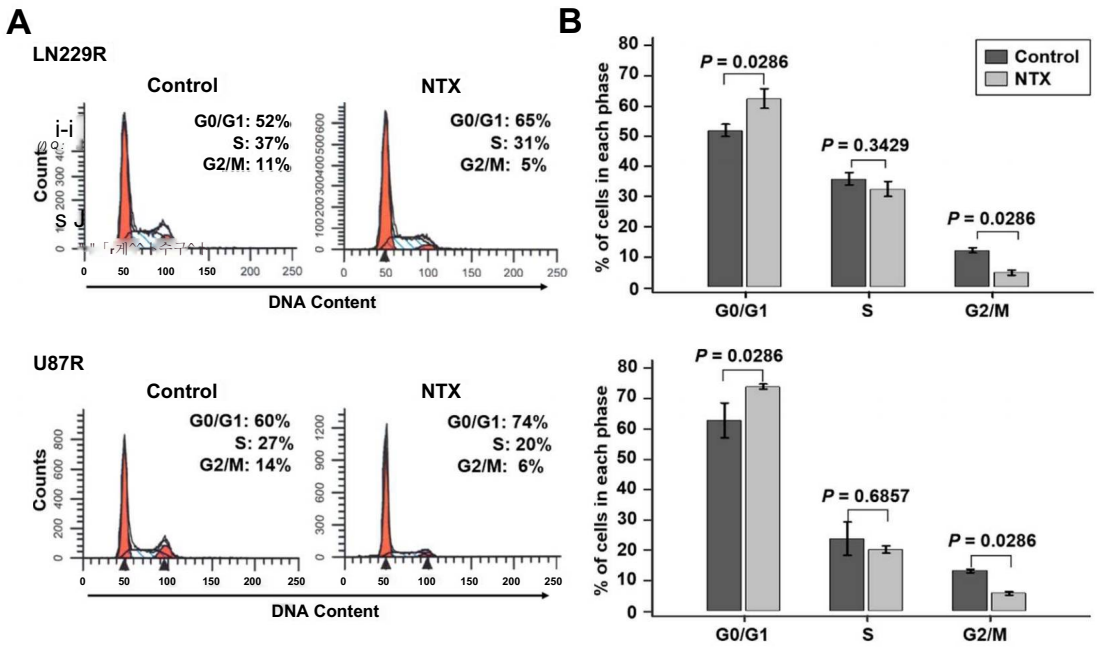

Figure 5. Effect of NTX treatment on cell-cycle. LN229R and U87R cells were treated with 10 // g/ml NTX for 24 hours, stained with propidium iodide and analyzed by fluorescence-activated flow cytometry. The percentages of the (A)LN229R and (B) U87R cell populations in the G0-G1 phase were significantly higher in the NTX-treated groups than the control groups (65% vs 52%, P = 0.0286, and 74% vs 60%, P = 0.0286, respectively), which suggested G0-G1 arrest. The quantitative data are expressed as the median with interquartile range of four independent experiments.

3.5 Effects of NTX treatment on cell-cycle regulatory proteins

To further investigate the association between cell cycle arrest and its regulatory proteins, I performed western blotting in NTX-treated TMZ-resistant cell lines. I observed that 10 /zg/ml NTX significantly decreased the protein expression levels of cyclin DI (LN229R*.P = 0.0286 ; U87R÷ P = 0.0286), phosphorylated Rb (LN229R : P = 0.0286 ; U87R : P = 0.0286), and cyclin A (LN229R÷ P = 0.0286 ; U87R- P = 0.0286), which are associated with G0/G1 arrest (Figure 6A & 6B). In investigating the association between the G2/M phase and its regulatory protein, I observed increased protein expression levels of CDK1 in both LN229R (P = 0.8852) and U87R (P = 0.0209) cells. Taken together, I found that the suppression of cell proliferation induced by NTX was caused by the induction of G0/G1 arrest. These results demonstrated that G0/G1 associated proteins controlled the cell cycle in both TMZ-resistant GBM cell lines.

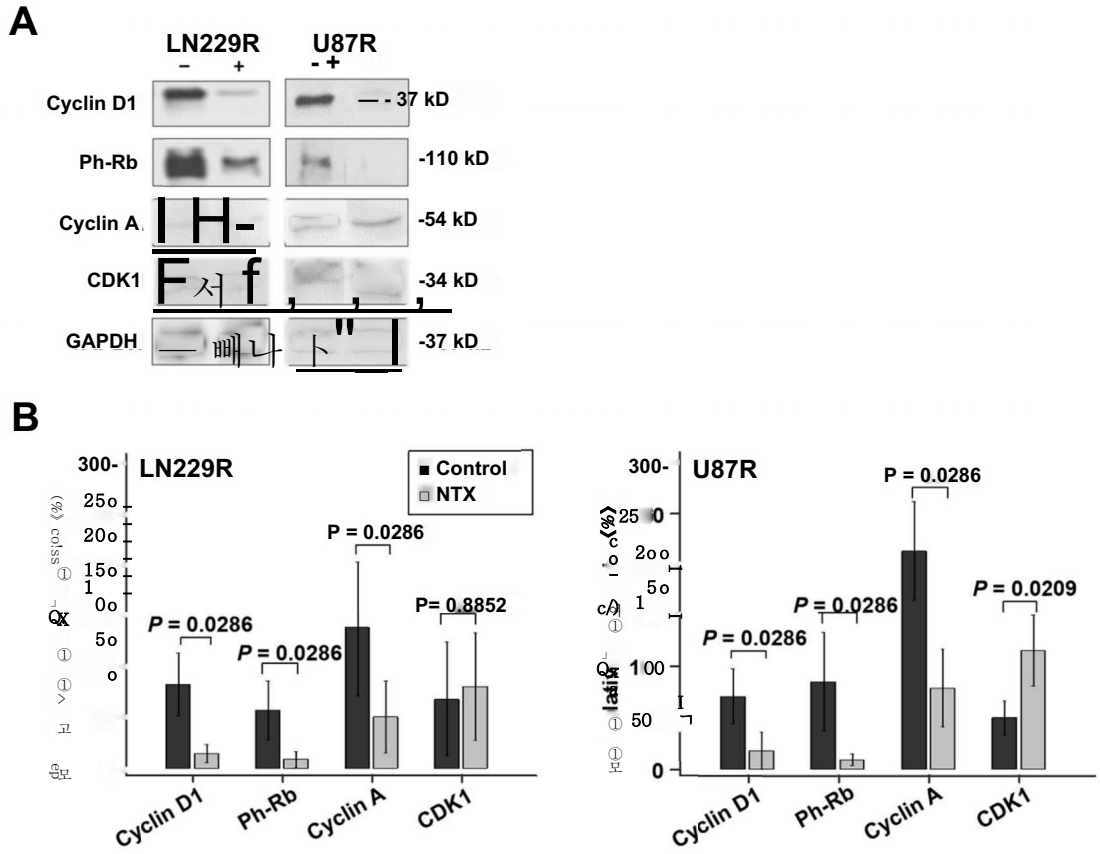

Figure 6. Effect of NTX treatment on cell-cycle regulatory proteins. LN229R and U87R cells were treated with 10 "g/ml NTX for 24 hours and harvested for the detection of the protein expression levels of cyclin DI, Ph—Rb, cyclin A and CDK1 by western blot analysis. The protein expression levels of cyclin DI, phosphorylated retinoblastoma and cyclin A were decreased after nitroxoline treatment in association with the G0-G1 arrest. The quantitative data are expressed as the median with interquartile range of four independent experiments.

3.6 NTX reduces APE-1 expression in TMZ-resistant GBM cells

Based on the in vitro results, I selected several genes [APE-1, MutS protein homolog 2 (MSH-2), MutS homolog 5 (MSH—6), O^6-alkylguanine DNA alkyl transferase (MGMT) and connexin 43 (Cx43)], all of which are known to be associated with TMZ-resistance, and we compared the expression levels of all the genes (Figure 7). Among them, only APE-1 showed an increased expression with statistical significance in both of the LN229R and U87R cell lines. The relative expression of APE-1 was found to be significantly increased in both TMZ-resistant cell lines compared to their respective parental cells: [LN229 : 0.9967% (IQR, 0.9402-1.0654), LN229R : 1.6590% (IQR, 1.6189-1.7294), P= 0.0286] and [U87 : 0.9700% (IQR, 0.9450-1.0600), U87R : 2.0150% (IQR, 1.9600-2.1450), P = 0.0209]. The expression of APE-1 was significantly decreased in both TMZ-resistant cell lines after 24 hours of NTX treatment ([LN229R : 1.6590% (IQR, 1.6189-1.7294), LN229R-NTX : 0.5435% (IQR, 0.5286-0.5686), P = 0.0286] and [U87R : 2.0150% (IQR, 1.9600-2.1450), U87R-NTX : 0.3500% (IQR, 0.2500-0.3600), P= 0.02091) (Figure 8).

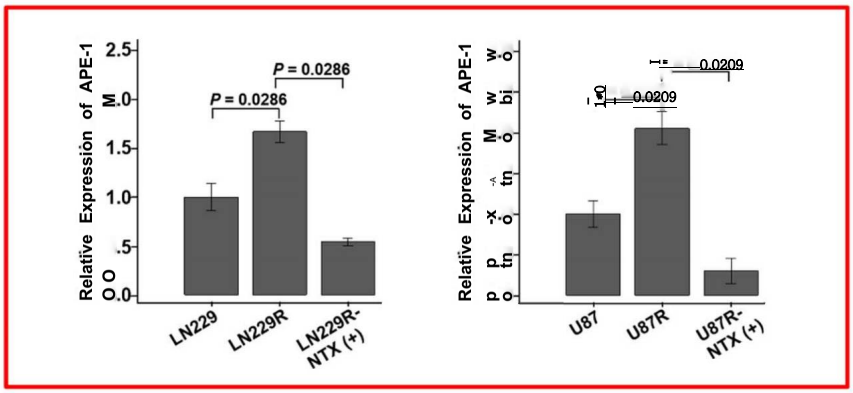
Relative Expression of APE-1
P = 0.0286
P = 0.0286
LN229
LN229R
LN229R-NTX (+)
Relative Expression of APE-1
0.0209
0.0209
U87
U87R
U87R-NTX (+)

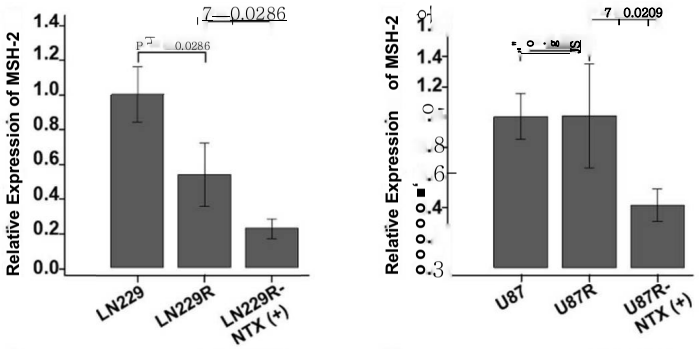
Relative Expression of MSH-2
LN229
LN229R
LN229R-NTX (+)
Relative Expression of MSH-2
0.0209
U87
U87R
U87R-NTX (+)

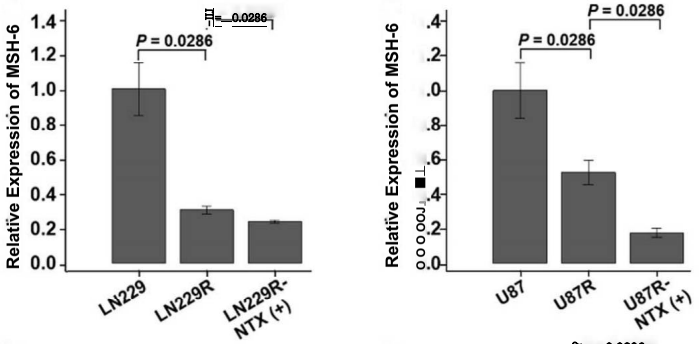
Relative Expression of MSH-6
P = 0.0286
P = 0.0286
LN229
LN229R
LN229R-NTX (+)
Relative Expression of MSH-6
P = 0.0286
P = 0.0286
U87
U87R
U87R-NTX (+)

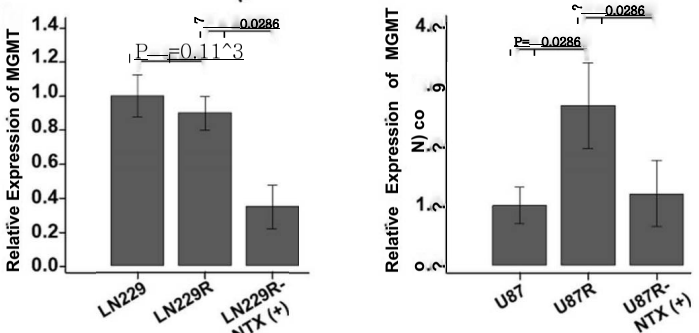
Relative Expression of MGMT
0.0286
LN229
LN229R
LN229R-NTX (+)
Relative Expression of MGMT
0.0286
0.0286
U87
U87R
U87R-NTX (+)

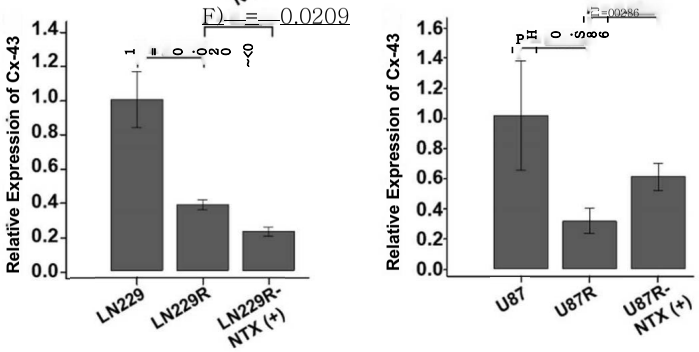
Relative Expression of Cx-43
0.0209
LN229
LN229R
LN229R-NTX (+)
Relative Expression of Cx-43
U87
U87R
U87R-NTX (+)

Figure 7. Effect of NTX treatment on the expression of genes related to TMZ resistance. The expression of APE-1 was increased in TMZ-resistant cells compared to their parental cells (LN229 vs LN229R- P = 0.0286 and U87 vs U87R- P = 0.0209), which was found to be significantly decreased after NTX treatment (LN229R vs LN229R-NTX : P= 0.0286 and U87R vs U87R-NTX : P = 0.0209). These patterns were observed identically in both cell lines only for the expression of APE—1. Note- LN229R = TMZ-resistant LN229, and U87R = TMZ-resistant U87.

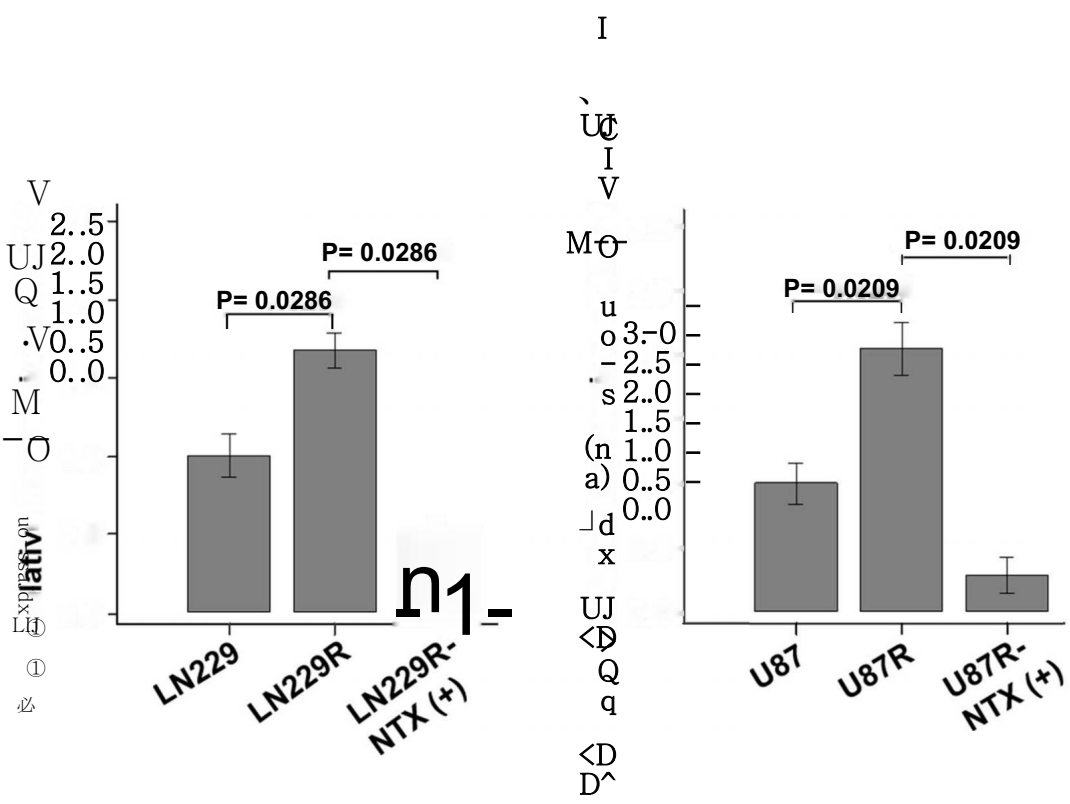

Figure 8. Analysis of APE-1 expression after NTX treatment. The relative expression of APE—1 was significantly increased in TMZ—resistant cell lines (LN229 vs LN229R, P= 0.0286 and U87 vs U87R, P= 0.0209) compared to the parental cell lines, which was significantly decreased after NTX treatment (LN229R vs LN229R-NTX, P= 0.0286 and U87 vs U87R-NTX, P= 0.0209) in both TMZ-resistant cell lines. Note: LN229R = TMZ—resistant LN229 and U87R = TMZ-resistant U87.

3.7 NTX triggers apoptosis in TMZ-resistant GBM cancer cells

The live and dead cell assay showed that 10 "g/ml NTX induced apoptosis, as demonstrated by the increased number of dead cell seen as red fluorescent cells in the images (Figure 9A). I observed that NTX significantly increased the number of dead cells in both the LN229R (P= 0.0209) and U87R (P= 0.0209) cell lines (Figure 9B). These data indicate that NTX treatment leads to the marked induction of apoptosis. To further confirm the apoptotic behavior induced by NTX, I investigated the levels of cleaved anti-PARP and cleaved caspase-3 by western blot analysis. In LN229R cells, the immunoblot analysis of the extracts of cells treated with 10, 20 and 40 "g/ml NTX showed significant increases in the protein expression levels of cleaved PARP compared with those of the untreated cells [10 //g/ml (P = 0.0304), 20 //g/ml (P = 0.0209), and 40 "g/ml (P = 0.0209)]. The increased protein expression of cleaved caspase 3 was detected in cells treated with 40 "g/ml NTX (P = 0.0209) (Figure 10A & 10B). In U87R cells, immunoblot analysis clearly showed statistically increased activation of cleaved PARP and cleaved caspase 3, even with low doses of NTX [cleaved PARP: 10 //g/ml (、P = 0.1939), 20 //g/ml (P= 0.0209) and 40 //g/ml (P= 0.0209)； cleaved caspase 3÷ 10 //g/ml (P = 0.0286), 20 //g/ml(*P* 0.0286) and 40 //g/ml (P = 0.0286)] (Figure 10C & 10D). These results confirmed that NTX induces apoptosis in both TMZ—resistant GBM cell lines.

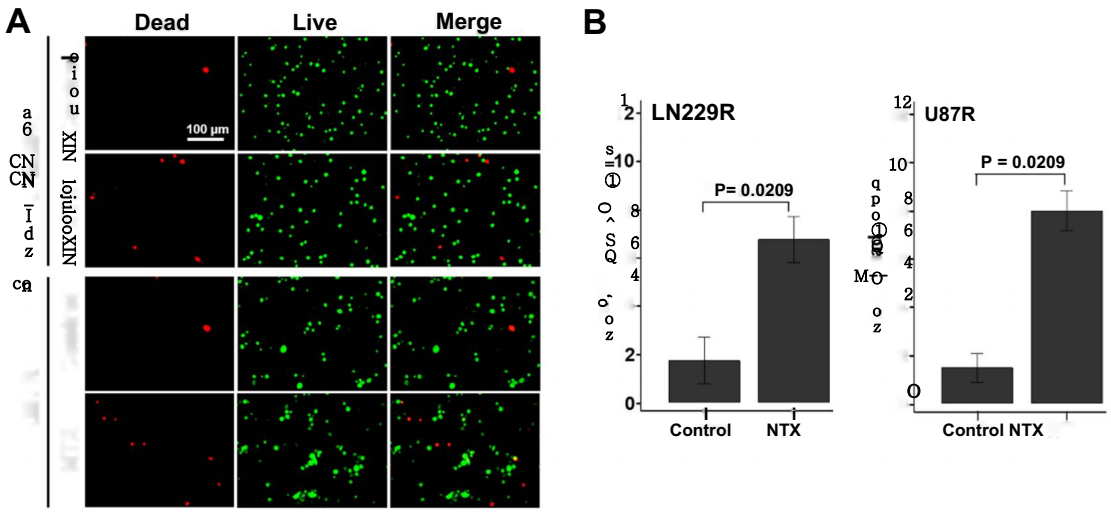

Figure 9. NTX triggers apoptosis in TMZ-resistant GBM cells by live and dead cell detection assay. (A) Fluorescence microscopy images of LN229R and U87R NTX-treated (10 //g/ml) or untreated cells, stained with the live and dead cell detection assay reagent. The scale bar is 100 //m at 200X. (B) There were significantly more dead cells in both TMZ—resistant GBM cell lines following NTX treatment than in the control groups. The quantitative data are expressed as the median with interquartile range of four independent experiments.

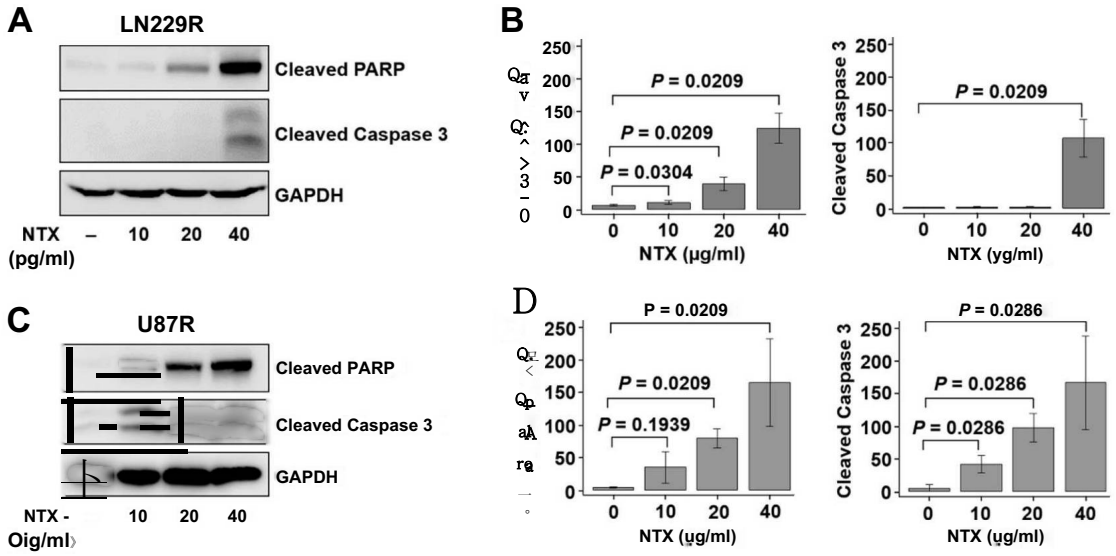

Figure 10. NTX triggers apoptosis in TMZ-resistant GBM cells. (A and C) LN229R cells ($1x10^5$) were cultured with 10, 20 and 40 // g/ml NTX for 24 hours. The protein expression levels of cleaved PARP and cleaved caspase-3 were detected after treatment with 40 "g/ml NTX in LN229R cells. (B and D) In U87R cells, PARP and cleaved caspase-3 proteins were detected after each dose of NTX. The data are presented as the median with interquartile range of four independent experiments.

3.8 NTX treatment of the TMZ-resistant GBM mouse model increases ADC value and survival

The in vivo MR study with a TMZ—resistant GBM mouse model was performed as shown in Figure 11A. Figure 1 IB represents the T2WI for anatomy and ADC maps for the response of treatment in both the control and NTX groups. The tumor volume ratio was significantly lower in the NTX group after 1—week of NTX treatment compared to the control group [control : 128.00% (IQR, 113.25-136.75), NTX : 97.00% (IQR, 87.75-101.25), P= 0.0122] (Figure 11C).

Tumor volume ratio = Tumor volume (post—2)/Tumor volume (post-1) X 100.

Moreover, a greater increase in the ADC ratio was observed in the NTX group than in the control group, which was detectable 1 week after the initiation of NTX treatment [control : 91.40% (IQR, 88.12-96.37), NTX : 110.00% (IQR, 108.00-115.25), P= 0.0079] (Figure 11D). However, there was no significant difference in tumor volume in the NTX group between post—1 and post-2 MRI [post-1 : 6.38 mm^2 (IQR, 5.15-7.54), post-2 : 6.03 mm^2 (IQR, 4.49-7.39), P = 0.3071], while the control group showed a significant increase in tumor volume between the two MRI scans [post-1: 4.57 mm^2 (IQR, 3.39-5.79), post-2: 5.62 mm^2 (IQR, 4.75 — 6.48), P= 0.0015]. In both the control and NTX groups, a significant decrease and increase in the ADC value were observed between the post-1 and post-2 MRI, respectively ([control÷ post-1: 8.05 x IO^{-4} mm^2/sec (IQR, 7.88 x 10^{-4}-8.36 x IO^{-4}), post-2 : 7.37 x 1◦—^{4} mm^2/sec (IQR, 7.19 x l(r^4-7.53 x 10^{-4}),P= 0.0163] and [NTX : post-1: 7.36 x 1◦—^{4} mm^2/sec (IQR, 6.71 x 10—^{4}-8.19 x IO^{-4}), post-2 : 8.23 x IO^{-4} mm^2/sec (IQR, 7.10 x 10" 4-9.10 x IO^{-4}), P = 0.0172]). In the long-term survival study, the NTX group

showed a significantly extended survival compared to the control group [mean : 72.8 days (95% CI, 68.7-76.9) vs 33.9 days (95% CI, 17.1-50.7), P= 0.0009, log-rank test] (Figure HE). I also investigated the third experimental group named as TMZ group, in which we treated our animal with TMZ for one more week after the confirmation of TMZ—resistant GBM mouse model (total time for TMZ injection : 2 weeks). As expected, I observed subsequent increased tumor volume and decreased ADC values after persistent TMZ treatment (Figure 12). Moreover, TMZ had no significant effect on long-term survival (Figure 12E) and hazard ratio for survival of all treatment group (Table 1).

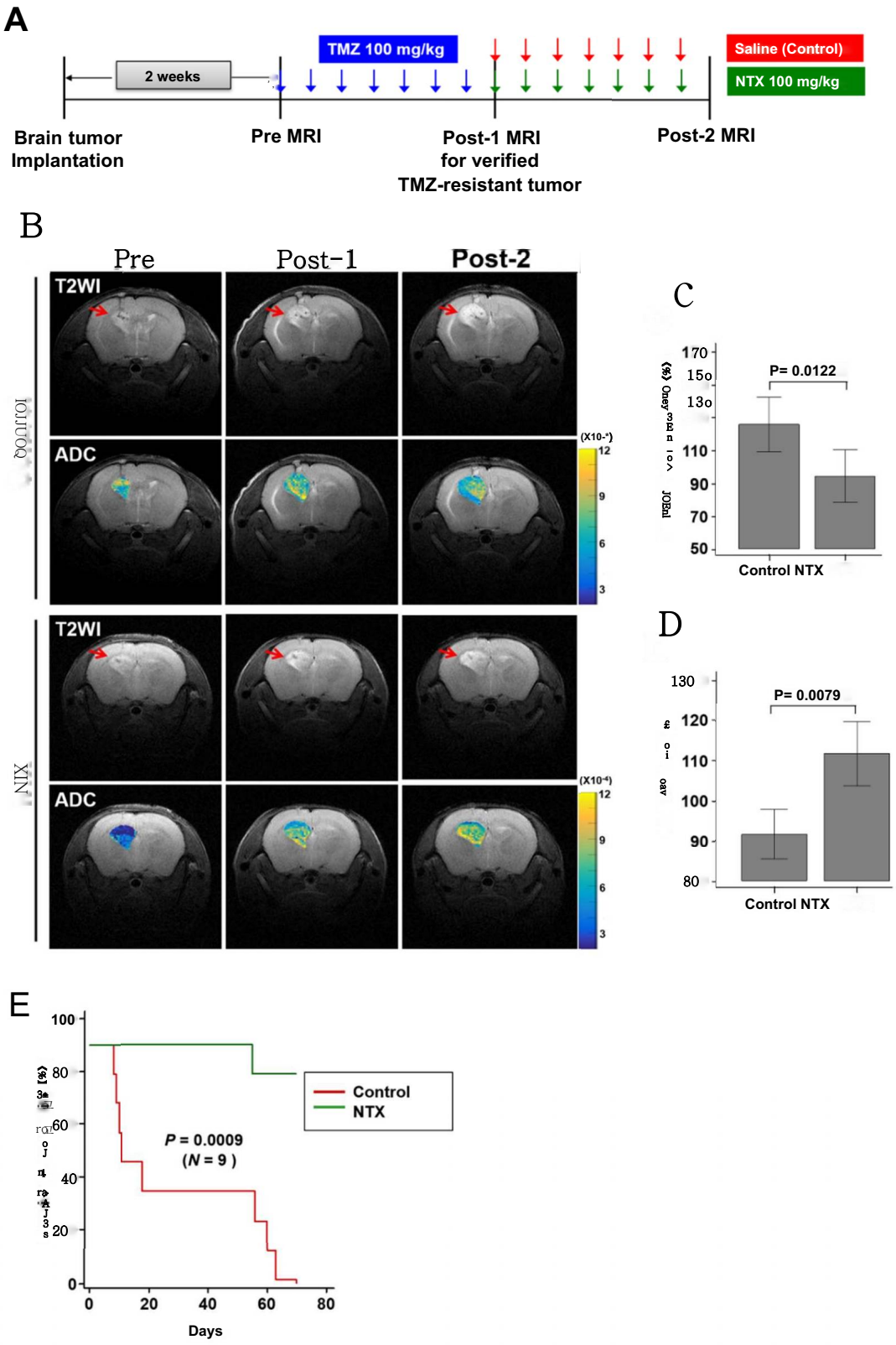

Figure 11. Short-term in vivo MR study and long-term survival analysis in a TMZ-resistant GBM mouse model. (A) The experimental design for the in vivo

MR study (、 n = 4, in each group). (B) Representative T2WI (1st row) and ADC maps (2nd row) for the control group and T2WI (3rd row) and ADC maps (4th row) for the NTX group, visualized with pretreatment MRI and post-1 MRI to verify TMZ resistance and with post-2 MRI to assess NTX effects. (C) The tumor volume ratio (%) was significantly decreased in the NTX group (P = 0.0122) compared to the control group. (D) The mean ADC ratio was significantly increased {P = 0.0079) in the NTX group. (E) The survival of the NTX group was significantly longer than that of the control group, which was analyzed by Kaplan-Meier survival analysis(n 9, in each group) [mean, 72.8 days (95% CI, 68.7-76.9) vs 33.9 days (95% CI, 17.1-50.7), P = 0.0009, log-rank test].

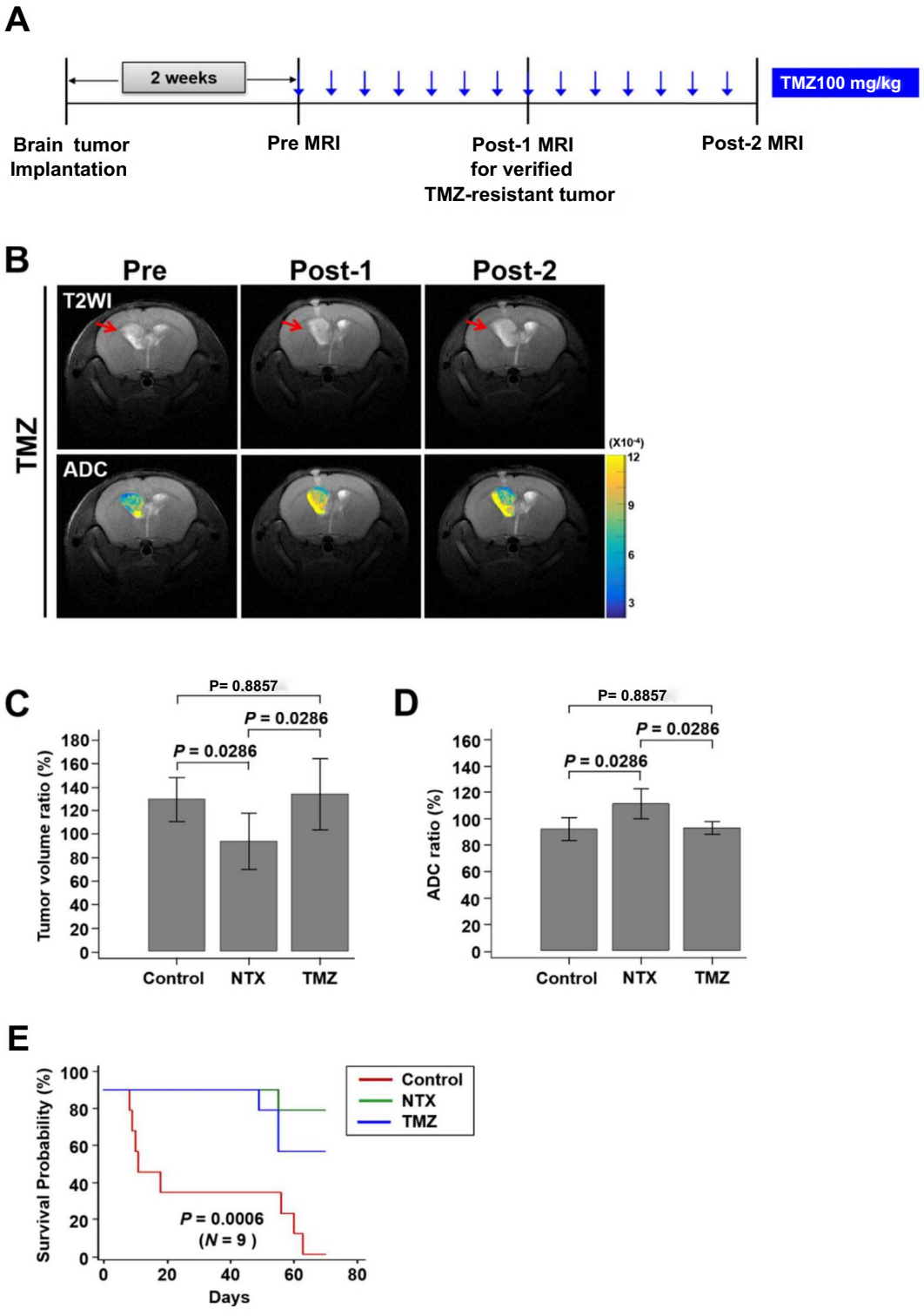

Figure 12. Short-term in vivo MR study and long-term survival analysis in a TMZ-resistant GBM mouse model for the TMZ group. (A) The experimental design for the in vivo study (n = 4, each). (B) MRI showed anatomical T2WI

and ADC maps. (C) The tumor volume ratio was significantly increased in the TMZ group compared to the NTX group (P= 0.0286). However, there was no significant difference between the tumor volume ratio of the TMZ group and the control group (P=0.8857). (D) The ADC ratio was significantly decreased in the TMZ group compared to the NTX group (P= 0.0286). However, there was no significant difference between the ADC ratio of the TMZ group and the control group (P = 0.8857). (E) A significant difference in survival rate was observed among the control, NTX, and TMZ groups [mean, 33.9 (95% CI, 17.1-50.7), 72.8 (95% CI, 68.7-76.9), and 64.3 (95% CI, 59.0-69.7) days ; P = 0.0006, log-rank test] (n = 9 in each group).

Table 1. Hazard ratio with 95% confidence interval for the survival of all treatment groups.

Group	Control	NTX	TMZ
Control	—	0.06778	0.2262
		(0.01526 - 0.3010)	(0.04947 - 1.0342)
NTX	14.7541	-	3.3371
	(3.3222 - 65.5252)		(0.9234 - 12.0609)
TMZ	4.4212	0.2997	-
	(0.9669 - 20.2163)	(0.08291 - 1.0830)	

3.9 APE-1 expression in the TMZ-resistant GBM mouse model was inversely correlated with the ADC value after NTX treatment

Figure 13A shows the histological analysis. In the case of H&E staining, for morphology and cellularity in tumors, a significant difference was observed in the NTX group compared to the control group [control: 100.00% (IQR, 100.00-100.00); NTX: 66.00% (IQR, 54.75-69.75), P = 0.0071] (Figure 13B). Moreover, the expression levels of Ki-67 [control: 100.00% (IQR, 100.00-100.00), NTX : 61.50% (IQR, 59.00-62.50), P= 0.0180] and APE-1 [control : 100.00% (IQR, 100.00-100.00), NTX : 70.00% (IQR, 62.00-73.00), P = 0.0180] were significantly decreased in the NTX group compared with the control group (Figure 13C & 13D). In the TUNEL assay for investigating DNA damage, a significantly increased number of apoptotic cells was observed after NTX treatment [control : 100.00% (IQR, 100.00-100.00), NTX : 212.00% (IQR, 155.00-247.25), P = 0.0071] when compared to the control group (Figure 13E). These results were validated by histology and agreed with the increased ADC value assessed by DWI. A significant inverse correlation was observed between the cellularity and the level of APE-1 and ADC [cellularity {R^2 = 0.71, P= 0.0089) and APE-1 {R^2 = 0.79, P= 0.0031)] in both the control and NTX groups (Figure 14A & 14B).

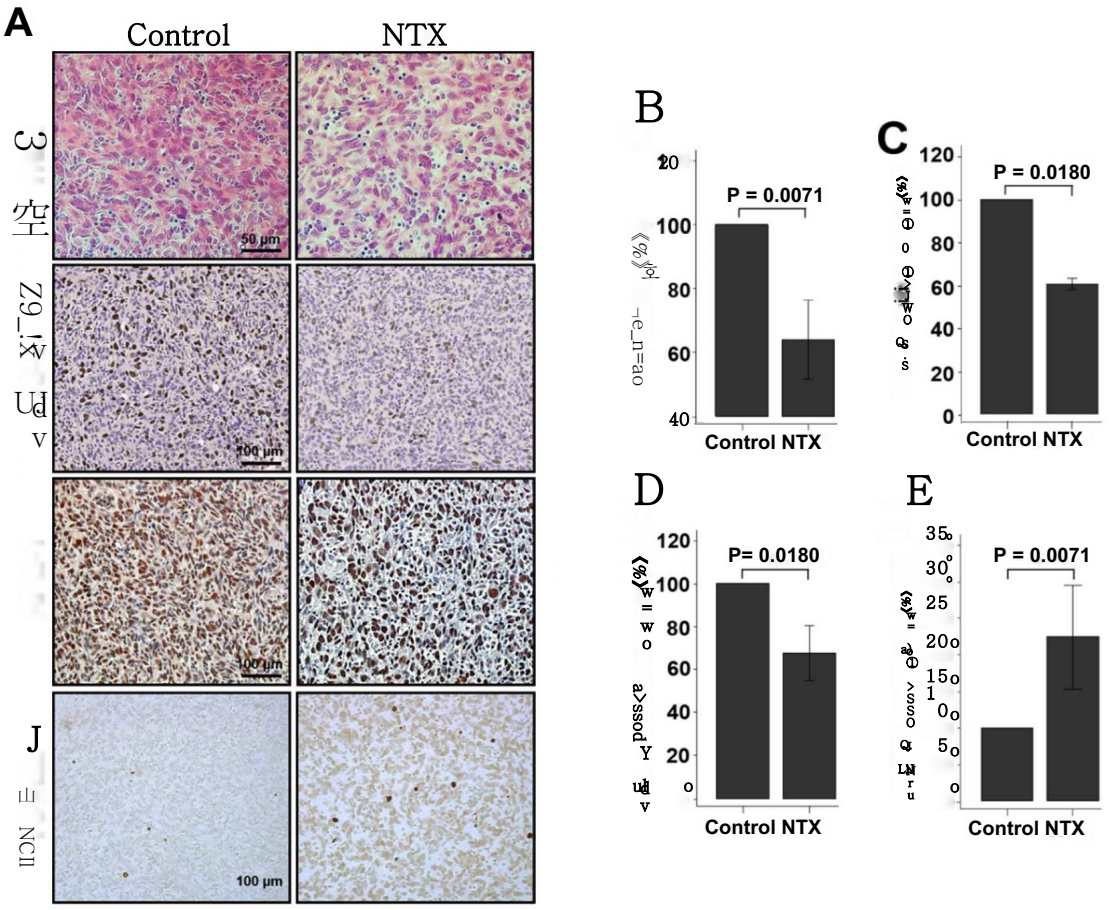

Figure 13. Histological analysis after NTX treatment. (A) Histological images representing hematoxylin and eosin (H & E) staining (1st row), immunohistochemistry images of Ki —67, (2nd row), APE-1 (3rd row) and TUNEL staining (4th row) for the control and NTX groups (X400 for H & E and x 200 for immunohistochemistry). (B-D) The cellularity (、P = 0.0071) evaluated by H&E, Ki-67 (P = 0.0180), and APE-1 (P = 0.0180) was significantly decreased in the NTX group compared to the control group. (E) Moreover, apoptotic cells, evaluated by TUNEL assay, were significantly increased in the NTX group {P = 0.0071).

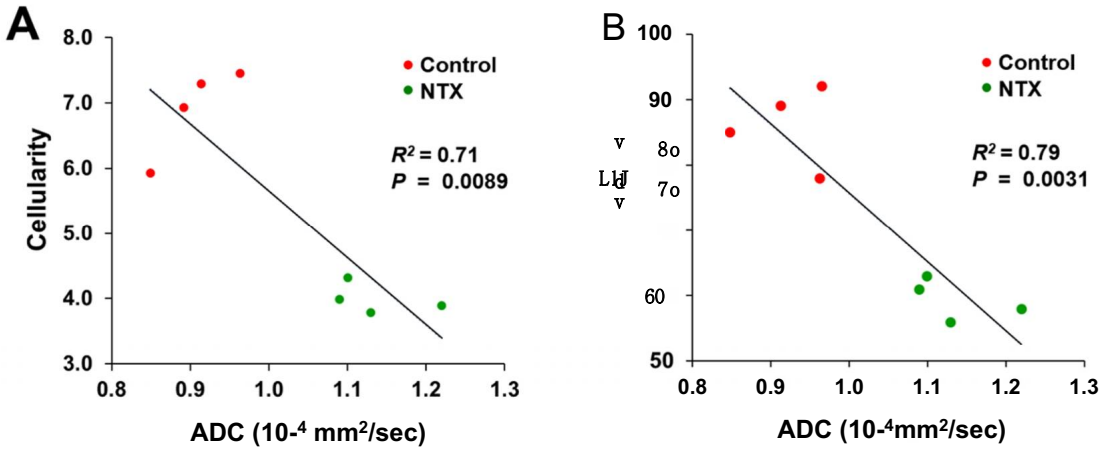

Figure 14. ADC Correlation with tumor cellularity and APE-1. (A) The tumor cellularity and (B) level of APE-1 showed a negative correlation with the ADC value (P = 0.0089, R^2 = 0.71) and (P = 0.0031, R^2 = 0.79), respectively, in both the control and NTX groups.

4. Discussion & conclusion

This study demonstrates that NTX can act as an anticancer compound against TMZ—resistant GBM through the in vitro and in vivo studies. First, NTX could reduce the expression of APE—1, an essential protein for DNA base excision repair and redox regulation, in TMZ-resistant GBM cells, which suggests that NTX increases the sensitivity of TMZ-resistant GBM cells to chemotherapy. Second, I observed an increase in the ADC value before a significant tumor volume change soon after NTX treatment in the TMZ-resistant GBM mouse model, which indicates a prior decrease in GBM cellularity before the shrinkage of tumor burden, as well as a long-term survival gain of NTX treatment in the TMZ-resistant GBM mouse model. Third, both APE—1 expression and tumor cellularity were inversely correlated with the ADC value after NTX treatment in the TMZ-resistant GBM mouse model, which suggests that DWI can be used as an imaging surrogate marker of early response to chemotherapy. I selected several genes related to TMZ-resistance through previous studies (9, 30, 34, 35) and investigated regulated the gene levels after NTX treatment in two TMZ-resistant cell lines. Interestingly, the increased APE-1 level of both TMZ-resistant cells compared to the parental cells was significantly decreased in TMZ-resistant cells after NTX treatment. This pattern was consistent with the morphological changes, which showed a recovery of cell morphology to parental cells after NTX treatment in both TMZ-resistant cell lines (Figure 4B & Figure 8). However, other genes including MSH-2, MSH-6, MGMT, and Cx43 did not show similar changes (Figure 7). APE-1 activity is elevated in human gliomas and confers resistance to ionizing radiation and alkylating agents

(13, 36). Previous study reported the use of a small molecule BER inhibitor potentiates the TMZ tumor cell killing and strongly sensitizes glioma cells to TMZ. Functional molecular studies of chemo—resistant human glioblastoma cell lines further demonstrated that by suppressing APE-1 activity, with antisense oligonucleotides or small interfering RNA (siRNA), TMZ cytotoxicity could be restored (13, 37). Another study reported that the siRNA directed against the APE-1 gene also led to decrease in cell proliferation, followed by induction of apoptosis (38) and that a downregulation of APE-1 is associated with the induction of DNA—damage through the increased expression of PARP (39). Related to these reports, my data showed an increased expression level of cleaved caspase-3 (CC3) and cleaved PARP, which are associated with the concentration of NTX in both TMZ—resistant cell lines (Figure 10). During preparation of TMZ-resistant cancer cells, I observed that the acquisition of TMZ-resistance affects cell morphology as the parental cells (U87 & LN229) were of round and polarized shape, which later transformed to elongated or spindle morphology (Figure 4A & 4B). Previous reports have revealed that the cytoskeleton is composed of 必 一 and B-tubulin, which form the microtubules that are required for cell differentiation and the maintenance of structural integrity (40). In addition, the migrative and invasive properties of GBM cells were found to be potentially blocked by a microtubule inhibitor (41). It is also obvious that the migrative and invasive features of GBM cells contribute to the development of resistance to apoptosis (42, 43). In agreement with previous reports, by the use of immunofluorescence staining, I found that NTX disrupted the microtubule structures of both TMZ-resistant GBM cell lines, leading to

impairment of the colony formation capacity and the migrative and invasive properties of cancer cells. Based on these findings, the downregulation APE-1 by NTX was able to increase the therapeutic effect against TMZ resistance, which can be supported by the reduced colony formation and migration capacities after NTX treatment as well (Figure 3). This morphological transformation process resembles with epithelial to mesenchymal transition (EMT), the process that transfigure epithelial cells into mesenchymal cells. During cancer progression, after EMT activation, tumor epithelial cells lose their cell polarity and cell-cell adhesion and gain migratory and invasive properties and become mesenchymal cell types and the expression of markers related to EMT (E—cadherin) is lost, while the expression of markers associated with mesenchymal states is activated (N-cadherin and Vimentin). Previous studies reported that cells that undergoes epithelial to mesenchymal transition become more invasive, with increased migratory properties and exhibits resistance to several chemotherapeutic agents (44). Wang et. al. showed the close link between the enhanced migration capacity of cells, acquired epithelial-mesenchymal transition and level of TMZ—resistance in glioma cells (45). In my study, as I already mentioned, I observed the recovery of cell morphology of both TMZ-resistant cancer cell line (from long and spindle to oval and Polaroid shape) after NTX treatment, which ultimately results G0-G1 arrest and decreased expression of cell cycle regulatory proteins (cyclin DI and Rb) in both TMZ-resistant GBM cell lines. I speculate that there might be a probability of the involvement of EMT phenomena in TMZ-resistant cell lines. As the cancers are heterogeneous in nature, future drug discovery efforts

directed at enhancing patient survival will undoubtedly need to consider the plasticity of cancer cells and one source of such plasticity is EMT pathway. Therefore, it would be interesting to investigate the role of NTX in EMT phenomena for TMZ—resistance GBM and this study provided the platform for future prospective. In case of in vivo study, we can explore the EMT markers after TMZ treatment to confirm TMZ—resistance and after NTX treatment to check the response of NTX on TMZ-resistance through EMT pathway.

To investigate the therapeutic effect of TMZ resistant GBM by NTX in vivo, I developed a TMZ-resistant GBM-bearing mouse model (30-32) and assessed cellularity changes using the ADC parameter respectively (46). In my study, the TMZ-resistant GBM-bearing mouse model was confirmed by investigating the tumor size and ADC value after TMZ treatment for 1 week. All control, NTX, and TMZ groups showed an increased tumor size which indicates the development of resistance even after TMZ. In our present study, to assess the early therapeutic effect of NTX against TMZ-resistant GBM, I measured changes in tumor volume and ADC values, where I observed a more prominent ADC increase of TMZ-resistant GBM in the NTX group than control group, which was prior to the tumor volume decrease. I also confirmed the long-term survival gain of NTX in the TMZ-resistant GBM model as well. These results suggest that NTX has a potent anti-tumor activity even within the early period, which resulted in the extended survival of the TMZ-resistant GBM model. One might assume that the 1-week TMZ exposure may be insufficient to develop a TMZ-resistant GBM model. To further scrutinize this possibility, I investigated the TMZ group, which was given TMZ for one more week after the confirmation

of a TMZ-resistant GBM-bearing mouse model (total time TMZ received- 2 weeks), and I also observed subsequent increased tumor volume and decreased ADC values after persistent TMZ treatment (Figure 12). This finding clearly reflects that GBM had further progressed as resistance developed to TMZ in the TMZ group (47, 48). The ADC changes after NTX treatment were also correlated with the histological findings including significantly decreased cellularity and cell proliferation in the NTX group of the TMZ-resistant GBM model compared with the control group (Figure 13), which are, in particular, supported by the decreased APE-1 expression level and the increased TUNEL-positive cells, well correlated with the in vitro results in my study (Figure 8, 13, 14 and 10). Moreover, numerical data of cellularity change after NTX treatment by H&E which were consistent with a previous report (49) and the APE—1 expression change by immunohistochemistry were negatively correlated with the ADC value in both the control and NTX groups (Figure 14). This demonstrated that the ADC value could be used as a noninvasive biomarker to evaluate the early treatment effect of NTX in TMZ-resistant GBM, which could result in long-term survival gain. NTX is administered orally, the standard dose of NTX used to treat urinary tract infections is 750 mg/day (16). In my study, I administetred 100 mg/kg/day of NTX in our nude mice, which is far less as compared to common dose (750 mg/day) used for human UTI treatment (37). This study has a limitation. In a TMZ-resistant GBM mouse model, I used a limited number of mice in each group for the evaluation of an early response to NTX as well as long-term survival to minimize the animal number according to the guideline of the institutional animal care and use committee in our institute.

Conclusion

In conclusion, I have demonstrated that the NTX could induce apoptosis through the decreased expression of APE—1 in TMZ-resistant GBM, inhibiting cell migration and proliferation in vitro and inhibit the growth of a TMZ-resistant GBM tumor model, which is confirmed by a decreased tumor volume and an increased ADC after short-term NTX therapy in addition to extended survival. Particularly, since MGMT is overexpressed in ~70% of GBM, this study supports that NTX is a promising candidate for future clinical trials against TMZ-resistant GBM as a second-line treatment regimen.

Bibliography

1. Kleihues P, Louis DN, Scheithauer BW, Rorke LB, Reifenberger G, Burger PC, et al. The WHO classification of tumors of the nervous system. J NeuropatholExp Neurol. 2002 ; 61 (3)·*215-25 ; discussion 26 — 9.

2. Stupp R, Mason WP, van den Bent MJ, Weller M, Fisher B, Taphoorn MJ, et al. Radiotherapy plus concomitant and adjuvant temozolomide for glioblastoma. N Engl J Med. 2005;352(10):987-96.

3. Wolf A, Agnihotri S, and Guha A. Targeting metabolic remodeling in glioblastoma multiforme. Oncotarget. 2010 ; 1 (7) - 552-62.

4. Stupp R, Hegi ME, Mason WP, van den Bent MJ, Taphoorn MJ, Janzer RC, et al. Effects of radiotherapy with concomitant and adjuvant temozolomide versus radiotherapy alone on survival in glioblastoma in a randomised phase III study÷ 5-year analysis of the EORTC-NCIC trial. Lancet Oncol. 2009 ; 10(5) : 459-66.

5. Hegi ME, Diserens AC, Gorlia T, Hamou MF, de Tribolet N, Weller M, et al. MGMT gene silencing and benefit from temozolomide in glioblastoma. NEngl J Med. 2005 ; 352(10) : 997-1003.

6. Park CK, Kim JE, Kim JY, Song SW, Kim JW, Choi SH, et al. The Changes in MGMT Promoter Methylation Status in Initial and Recurrent Glioblastomas. Transl Oncol. 2012 ; 5 (5) -393 — 7.

7. van Nifterik KA, van den Berg J, van der Meide WF, Ameziane N, Wedekind LE, Steenbergen RDM, et al. Absence of the MGMT protein as well as methylation of the MGMT promoter predict the sensitivity for temozolomide. Brit J Cancer. 2010;103 (1) :29_35.

8. Kanzawa T, Bedwell J, Kondo Y, Kondo S, and Germano IM. Inhibition of DNA repair for sensitizing resistant glioma cells to temozolomide. JNeurosurg. 2003 ; 99(6) : 1047-52.

9. Zhang J, Stevens MF, and Bradshaw TD. Temozolomide- mechanisms of action, repair and resistance. Curr Mol Pharmacol. 2012;5(l):102_14.

10. Almeida KH, and Sobol RW. A unified view of base excision repair : lesion-dependent protein complexes regulated by post-translational modification. DNA Repair (Amst). 2007 ; 6 (6)·- 695 — 711.

11. Trivedi RN, Almeida KH, Fornsaglio JL, Schamus S, and Sobol RW. The role of base excision repair in the sensitivity and resistance to temozolomide-mediated cell death. Cancer Res. 2005 ; 65 (14) *6394—400.

12. Bobola MS, Emond MJ, Blank A, Meade EH, Kolstoe DD, Berger MS, et al. Apurinic endonuclease activity in adult gliomas and time to tumor progression after alkylating agent-based chemotherapy and after radiotherapy. Clin Cancer Res. 2004 ; 10(23) : 7875-83.

13. Silber JR, Bobola MS, Blank A, Schoeler KD, Haroldson PD, Huynh MB, et al. The apurinic/apyrimidinic endonuclease activity of Apel/Ref-1 contributes to human glioma cell resistance to alkylating agents and is elevated by oxidative stress. Clin Cancer Res. 2002 ; 8 (9) *3008-18.

14. Sleire L, Forde HE, Netland IA, Leiss L, Skeie BS, and Enger PO. Drug repurposing in cancer. Pharmacol Res. 2017;124:74-91.

15. Hernandez JJ, Pryszlak M, Smith L, Yanchus C, Kurji N, Shahani VM, et al. Giving Drugs a Second Chance- Overcoming Regulatory and Financial Hurdles in Repurposing Approved Drugs As Cancer Therapeutics. Front Oncol.

2017 ; 7 : 273.

16. Naber KG, Niggemann H, Stein G, and Stein G. Review of the literature and individual patients* data meta-analysis on efficacy and tolerance of nitroxoline in the treatment of uncomplicated urinary tract infections. BMC Infect Dis. 2014 ; 14 : 628.

17. Shim JS, Matsui Y, Bhat S, Nacev BA, Xu J, Bhang HE, et al. Effect of nitroxoline on angiogenesis and growth of human bladder cancer. J Natl Cancer Inst. 2010 ; 102(24) : 1855-73.

18. Sato Y. Role of aminopeptidase in angiogenesis. Biol Pharm Bull. 2004;27(6):772-6.

19. Brooks CL, and Gu W. How does SIRT1 affect metabolism, senescence and cancer? Nat Rev Cancer. 2009;9 (2) :123_8.

20. Mohamed MM, and Sloane BF. Cysteine cathepsins- multifunctional enzymes in cancer. Nat Rev Cancer. 2006 ; 6 (10)-764-75.

21. Mirkovic B, Markelc B, Butinar M, Mitrovic A, Sosic I, Gobec S, et al. Nitroxoline impairs tumor progression in vitro and in vivo by regulating cathepsin B activity. Oncotarget. 2015 ; 6 (22) : 19027-42.

22. Lazovic J, Guo L, Nakashima J, Mirsadraei L, Yong W, Kim HJ, et al. Nitroxoline induces apoptosis and slows glioma growth in vivo. Neuro-Oncology. 2015;17 (1) :53 — 62.

23. Chang WL, Hsu LC, Leu WJ, Chen CS, and Guh JH. Repurposing of nitroxoline as a potential anticancer agent against human prostate cancer - a crucial role on AMPK/mTOR signaling pathway and the interplay with Chk2 activation. Oncotarget. 2015 ; 6 (37) -39806-20.

24. Xu N, Huang L, Li X, Watanabe M, Li C, Xu A, et al. The Novel Combination of Nitroxoline and PD—1 Blockade, Exerts a Potent Antitumor Effect in a Mouse Model of Prostate Cancer. Int J Biol Sci. 2019 ; 15 (5) - 919 —28.

25. Galban CJ, Hoff BA, Chenevert TL, and Ross BD. Diffusion MRI in early cancer therapeutic response assessment. NMR Biomed. 2017 ; 30(3).

26. Malayeri AA, El Khouli RH, Zaheer A, Jacobs MA, Corona—Villalobos CP, Kamel IR, et al. Principles and Applications of Diffusion—weighted Imaging in Cancer Detection, Staging, and Treatment Follow-up. Radiographics. 2011 ; 31(6) : 1773-91.

27. Tourell MC, Shokoohmand A, Landgraf M, Holzapfel NP, Poh PSP, Loessner D, et al. The distribution of the apparent diffusion coefficient as an indicator of the response to chemotherapeutics in ovarian tumour xenografts. Sci Rep-Uk. 2017 ; 7.

28. Le Bihan D, and lima M. Diffusion Magnetic Resonance Imaging: What Water Tells Us about Biological Tissues. Pios Biol. 2015 ; 13(7).

29. Sugahara T, Korogi Y, Kochi M, Ikushima I, Shigematu Y, Hirai T, et al. Usefulness of diffusion-weighted MRI with echo—planar technique in the evaluation of cellularity in gliomas. Jmri-JMagn Reson Im. 1999 ; 9 (1) *53-60.

30. Lee SY. Temozolomide resistance in glioblastoma multiforme. Genes Dis. 2016 ; 3(3) : 198-210.

31. Oliva CR, Nozell SE, Diers A, McClugage SG, Sarkaria JN, Markert JM, et al. Acquisition of Temozolomide Chemoresistance in Gliomas Leads to Remodeling of Mitochondrial Electron Transport Chain. J Biol Chem. 2010 ; 285(51) : 39759-67.

32. Clarke MJ, Mulligan EA, Grogan PT, Mladek AC, Carlson BL, Schroeder MA, et al. Effective sensitization of temozolomide by ABT—888 is lost with development of temozolomide resistance in glioblastoma xenograft lines. Mol Cancer Ther. 2009 ; 8(2) : 407-14.

33. Yeom SY, Nam DH, and Park C. RRAD promotes EGFR-mediated STAT3 activation and induces temozolomide resistance of malignant glioblastoma. Mol Cancer Ther. 2014 ; 13 (12) : 3049-61.

34. Hudson AL, Parker NR, Khong P, Parkinson JF, Dwight T, Ikin RJ, et al. Glioblastoma Recurrence Correlates With Increased APE1 and Polarization Toward an Immuno-Suppressive Microenvironment. Frontiers in Oncology. 2018 ; 8.

35. McFaline-Figueroa JL, Braun CJ, Stanciu M, Nagel ZD, Mazzucato P, Sangaraju D, et al. Minor Changes in Expression of the Mismatch Repair Protein MSH2 Exert a Major Impact on Glioblastoma Response to Temozolomide. Cancer Res. 2015 ; 75 (15) : 3127~38.

36. Tell G, Fantini D, and Quadrifoglio F. Understanding different functions of mammalian AP endonuclease (APE1) as a promising tool for cancer treatment. Cell Mol Life Sei. 2010 ; 67(21) : 3589-608.

37. Montaldi AP, Godoy PR, and Sakamoto—Hojo ET. APE1/REF—1 down-regulation enhances the cytotoxic effects of temozolomide in a resistant glioblastoma cell line. MutatRes Genet Toxicol Environ Mutagen. 2015;793:19 — 29.

38. Hong J, Chen Z, Peng DF, Zaika A, Revetta F, Washington MK, et al. APE1-mediated DNA damage repair provides survival advantage for

esophageal adenocarcinoma cells in response to acidic bile salts. Oncotarget. 2016 ; 7(13) : 16688-702.

39. Fung H, and Demple B. A vital role for Apel/Refl protein in repairing spontaneous DNA damage in human cells. Mol Cell. 2005 ; 17 (3) : -463-70.

40. Hammond JW, Cai DW, and Verhey KJ. Tubulin modifications and their cellular functions. Curr Opin Cell Biol. 2008;20(l) :71 — 6.

41. Henry WI, Dubois J, and Quick QA. The microtubule inhibiting agent epothilone B antagonizes glioma cell motility associated with reorganization of the actin-binding protein alpha—actinin 4. Oncol Rep. 2011 ; 25 (3) : -887-93.

42. Lefranc F, Brotchi J, and Kiss R. Possible future issues in the treatment of glioblastomas: Special emphasis on cell migration and the resistance of migrating glioblastoma cells to apoptosis. Journal of Clinical Oncology. 2005 ; 23(10) : 2411-22.

43. Lefranc F, Facchini V, and Kiss R. Proautophagic drugs* A novel means to combat apoptosis-resistant cancers, with a special emphasis on glioblastomas. Oncologist. 2007 ; 12 (12) : 1395-403.

44. Singh A, and Settleman J. EMT, cancer stem cells and drug resistance- an emerging axis of evil in the war on cancer. Oncogene. 2010 ; 29 (34) : 4741-51.

45. Wang JJ, Zhou FG, Li Y, Li QS, Wu ZC, Yu LL, et al. Cdc20 overexpression is involved in temozolomide—resistant glioma cells with epithelial-mesenchymal transition. Cell Cycle. 2017 ; 16 (24) : 2355-65.

46. Koral K, Mathis D, Gimi B, Gargan L, Weprin B, Bowers DC, et al. Common Pediatric Cerebellar Tumors- Correlation between Cell Densities and

Apparent Diffusion Coefficient Metrics. Radiology. 2013;268 (2) :532 — 7.

47. Zulfiqar M, Yousem DM, and Lai H. ADC Values and Prognosis of Malignant Astrocytomas* Does Lower ADC Predict a Worse Prognosis Independent of Grade of Tumor?—A Meta—Analysis. Am J Roentgenol. 2013 ; 200(3) : 624-9.

48. Pope WB, Lai A, Mehta R, Kim HJ, Qiao J, Young JR, et al. Apparent diffusion coefficient histogram analysis stratifies progression-free survival in newly diagnosed bevacizumab-treated glioblastoma. AJNR Am J Neuroradiol. 2011 ; 32(5) : 882-9.

49. Pope WB, Qiao XJ, Kim HJ, Lai A, Nghiemphu P, Xue X, et al. Apparent diffusion coefficient histogram analysis stratifies progression-free and overall survival in patients with recurrent GBM treated with bevacizumab- a multi-center study. J Neuro - Oncol. 2012 ; 108 (3) -491-8.

초록

배경: 교모세포종은 가장 예후가 나쁜 악성 뇌종양 중 하나이며 가장 치료가 어려운 종양 중 하나이다. 현재 교모세포종 치료의 표준은 안전한 수술적 절제를 포함하여 방사선 치료와 화학 치료이다.

화학치료법에서 테모졸로마이드 (TMZ) 를 이용한 치료는 교모세포종 환자에게는 표준 치료이다. 그러나 복구 단백질 06_me^iylguanine—DNA methyltransferase (MGMT) 의 발현이 높아지거나 Mismatch repair (MMR) pa比iway의 부재 때문에 TMZ로 유도되는 DNA lesion O6-methylguanine의 의해 생기는 세포 독성 효과에 내성을 가지게 되는 경우가 종종 발생한다. TMZ로 유도되는 세포 독성 효과의 타겟은 N7-methyleguanine and N3-methyleadenine 의 다수는 Base excision repair(BER) 기질들인데, 이러한 DNA병변들은 쉽게 복구된다. 그러므로 BER 단백질들은 TMZ내성을 극복하기 위한 중요한 대상이 된다. 본 연구에서는 BER 경로와 관련된 다기능성 효소인 apurinic/apy rimidinic endonuclease-1 (APE-lX 초첨을 맞추었다.

재료 및 방법: 본 연구자는 in w간7?상에서 TMZ내성 세포를 생산하여 집락형성 분석법 (clonogenic assay)과 세포 이동 분석법 (migration assay)를 통해 나이트로졸린 (NTX)의 치료적 효과를 평가해보았다. TMZ내성 세포주에서 NTX 처리 전 후에 TMZ내성 연관 단백질의 발현 정도를 정량 실시간 중합효소 연쇄 반응을 통해 확인하였으며 in i次/지실험으로 유세포 분석과 웨스턴 블랏을 진행하였다. In in vivo 실험에서는 TMZ내성 GBM 마우스 모델로 ADC값 변화와 종양 크기 각각의 변화를 평가하기위해 9.4T MRI를 통해 T2WI와 DWI데이터를 얻었다. 마지막으로 ADC값과 조직학적 결과의 관계 분석을 위해 조직학적 분석과 회귀분석을 수행하였다.

결과: 본 연구자는 TMZ내성 세포에서 세포사멸을 유발하는 NTX의 처치 후

APE-1 의 발현이 현저하게 감소하는 것을 관찰했다. 또한 NTX가 TMZ내성 세포의 군집 형성 능력과 이동 능력을 현저히 감소시키는 것을 관찰했다. In in vivo 실험에서는 NTX가 TMZ내성 GBM 마우스 모델에서 종양 크기를 감소시키고 종양 크기가 감소하기 전 NTX를 처치하지 않은 대조군과 비교하여 NTX처치군에서 ADC 값이 증가하는 결과를 확인하였다. TMZ내성 GBM에서 NTX에 의한 APE-1의 발현 감소는 치료효과로 이어지고 ADC값과 역상관관계를 가지며 이는 NTX 치료 동물에서 더 오래 생존하는 결과를 보여준다.

결론: NTX는 in vitro 상에서 TMZ내성 GBM의 APE-1 의 발현을 감소시켜 세포사멸을 유도하고 TMZ내성 GBM 종양 모델의 성장을 억제할 수 있다. 따라서 NTX는 TMZ내성 GBM에 대한 잠재적 치료 후보물질로 제시된다.

주요어: 테모졸로마이드 내성 교모세포종, DNA 복구 단백질, 아푸린/아피리미딘 염기 절제 수선 (BER), 엔도뉴클레아제-1(APE-1), 니트록솔린 (NTX), 확산 강조 영상 (DWI), 겉보기 확산계수 (ADC),

학 번: 2016-30782

본 논문의 결과 중 일부는 다음 논문에 게재되었음:

Hye Rim Cho* Nisha Kumari*, Nishant Thakur, Hien Thi Vu, Hyeonjin Kim, Seung Hong Choi. Decreased APE-1 by Nitroxoline Enhances Therapeutic effects in a temozolomide-resistant Glioblastoma: Correlation with diffusion-weighted imaging. Scientific Reports 2019-12 ; 16613.

본 논문의 결과 중 일부는 다음 학회에서 발표됨:

22nd Annual meeting and education day of the Society for Neurooncology,

November2017, Marriott Marquis, San Francisco, California. DDIS-04

Nitroxoline exhibit anticancer activity inducing apoptosis in a temozolomide-resistant glioblastoma. Neuro-oncology, 06 Nov 2017, 19 (Suppl 6) :vi59—vi59.